Received: 29 July 2022 | Revised: 10 October 2022 | Accepted: 11 October 2022

DOI: 10.1111/apha.13896

ACTA PHYSIOLOGICA

RESEARCH PAPER

The cold-sensing ion channel TRPM8 regulates central and peripheral clockwork and the circadian oscillations of body temperature

Alfonso Reimúndez[1] | **Carlos Fernández-Peña**[2,3] | **Purificación Ordás**[2] | **Pablo Hernández-Ortego**[2] | **Rosalía Gallego**[4] | **Cruz Morenilla-Palao**[2] | **Juan Navarro**[1] | **Francisco Martín-Cora**[1] | **José Luís Pardo-Vázquez**[5] | **Lindsay A. Schwarz**[3] | **Victor Arce**[1] | **Félix Viana**[2] | **Rosa Señarís**[1]

[1]Department of Physiology, CIMUS, University of Santiago de Compostela, Santiago de Compostela, Spain

[2]Institute of Neuroscience. UMH-CSIC, Alicante, Spain

[3]St. Jude Children's Research Hospital, Memphis, Tennessee, USA

[4]Department of Morphological Sciences, University of Santiago de Compostela, Santiago de Compostela, Spain

[5]Department Physiotherapy, Medicine and Biomedical Sciences, CICA, University of A Coruña, A Coruña, Spain

Correspondence
Félix Viana, Institute of Neuroscience, UMH-CSIC, Alicante, Spain.
Email: felix.viana@umh.es

Rosa Señarís, Department of Physiology, CIMUS, University of Santiago de Compostela, Santiago de Compostela, Spain.
Email: rosa.senaris@usc.es

Present address
Alfonso Reimúndez, Institut de la Vision, Sorbonne Université, INSERM, CNRS, Paris, France

Funding information
Ministerio de Ciencia e Innovación, Grant/Award Number: RT2018- 099995- B100 to RS and AEI/10.13039/501100011033 to FV; Severo Ochoa Programme for Centres of Excellence; Generalitat Valenciana, Grant/Award Number: PROMETEO/2021/031; Ministerio de Universidades, Grant/Award Number: Margarita Salas postdoctoral fellowship to AR

Abstract

Aim: Physiological functions in mammals show circadian oscillations, synchronized by daily cycles of light and temperature. Central and peripheral clocks participate in this regulation. Since the ion channel TRPM8 is a critical cold sensor, we investigated its role in circadian function.

Methods: We used TRPM8 reporter mouse lines and TRPM8-deficient mice. mRNA levels were determined by in situ hybridization or RT-qPCR and protein levels by immunofluorescence. A telemetry system was used to measure core body temperature (Tc).

Results: TRPM8 is expressed in the retina, specifically in cholinergic amacrine interneurons and in a subset of melanopsin-positive ganglion cells which project to the central pacemaker, the suprachiasmatic nucleus (SCN) of the hypothalamus. TRPM8-positive fibres were also found innervating choroid and ciliary body vasculature, with a putative function in intraocular temperature, as shown in TRPM8-deficient mice. Interestingly, *Trpm8*$^{-/-}$ animals displayed increased expression of the clock gene *Per2* and vasopressin (AVP) in the SCN, suggesting a regulatory role of TRPM8 on the central oscillator. Since SCN AVP neurons control body temperature, we studied Tc in driven and free-running conditions.

See related editorial: Mishra SK, Gaddmeedhi S, 2023. A new role of TRPM8 in circadian rhythm and molecular clock. *Acta Physiol.* (Oxf). e13934.

[Correction added on December 3, 2022 after first online publication. The funding information has been updated.]

Alfonso Reimúndez, Carlos Fernández-Peña, and Purificación Ordás contributed equally to this work.

TRPM8-deficiency increased the amplitude of Tc oscillations and, under dim constant light, induced a greater phase delay and instability of Tc rhythmicity. Finally, TRPM8-positive fibres innervate peripheral organs, like liver and white adipose tissue. Notably, *Trpm8*$^{-/-}$ mice displayed a dysregulated expression of *Per*2 mRNA in these metabolic tissues.

Conclusion: Our findings support a function of TRPM8 as a temperature sensor involved in the regulation of central and peripheral clocks and the circadian control of Tc.

KEYWORDS

body temperature, central and peripheral clocks, circadian regulation, sensory physiology, TRPM8

1 | INTRODUCTION

Most physiological processes are governed by a circadian rhythm with a period of approximately 24 h. Such temporal organization has evolved in the presence of predictable environmental cues, principally daily cycles of light and temperature, generating temporal programs and resetting mechanisms, which are well conserved among different animal taxa.[1–3] Understanding how organisms detect these signals and synchronize molecular clocks in the brain and other tissues to the environment remains a central challenge in circadian research. The cellular and molecular mechanisms for synchronization to the daily light–dark cycles have been characterized in detail.[2,4] In mammals, a small subpopulation of retinal ganglion cells is intrinsically photosensitive (ipRGCs),[5] thanks to the expression of the photopigment melanopsin.[6,7] These neurons convey luminic information to the suprachiasmatic nucleus (SCN) in the hypothalamus, a bilateral collection of ~20 000 intrinsically rhythmic neurons considered the master biological pacemaker.[4] This central clock is daily reset by the light/dark retinal inputs and is responsible for sending time-of-day information to other areas of the central nervous system and to systemic tissues, which have their own, autonomous, peripheral clocks.[2,8]

The intrinsic circadian rhythmicity of the central and peripheral pacemakers is provided by a molecular clock machinery based on the oscillation of transcription factors and translation of genes and proteins, the so-called clock genes: *Clock* (Circadian Locomotor Output Cycles Kaput), *Bmal1* (Brain and Muscle Arnt-like), *Per* (Period1, 2, 3) and *Cry* (Cryptochrome1, 2).[9] Ultimately, their oscillatory activity generates circadian changes in the expression of clock-controlled genes (CCGs). One of the best-characterized CCGs in the SCN is the gene for the neuropeptide arginine vasopressin (AVP).[10] AVP-expressing neurons constitute one of the most important outputs of this hypothalamic nucleus and are involved in the regulation of many circadian functions, including body temperature.[11]

Light is the most powerful Zeitgeber for circadian functions. However, it has long been known that temperature cycles can also synchronize rhythms in both vertebrate and invertebrate organisms.[12–18] Nevertheless, our knowledge about how daily temperature fluctuations influence central and peripheral clocks is still rather limited. It has been classically considered that, differently to the response to light, central clock machinery is buffered against changes in clock period length induced by temperature, a phenomenon known as temperature compensation.[19,20] On the contrary, peripheral oscillators are exquisitely sensitive to thermal stimuli.[20] This differential response to temperature between central and peripheral clocks would allow the SCN to drive circadian rhythms in body temperature, which would then act as a universal internal entrainment signal to cell-autonomous peripheral oscillators throughout the body. The molecular identity of the thermal sensors involved in the regulation of circadian clocks by temperature is still unknown. Recent studies in *Drosophila* have described that temperature input to the brain clock appears to rely mainly on the peripheral sensory nervous system of the fly and that different families of thermoreceptive molecules might be involved, including ionotropic receptors (IRs) and TRP channels.[21]

The transient receptor potential melastatin 8 (TRPM8) channel is the most important cold sensor in mammals[22,23] and plays a very relevant role in thermoregulation and energy homeostasis.[24–26] Indeed, deletion of TRPM8 in mice induces a defective thermoregulation and the development of late-onset obesity.

In this study, we demonstrate that TRPM8 is also involved in central and peripheral clockwork and in the circadian regulation of Tc. TRPM8 is expressed in specific neurons in the retina and TRPM8-positive fibres project

to the SCN regulating SCN clock and neuropeptide levels, contributing to the fine-tuning of circadian body temperature oscillations. Finally, we found that TRPM8 sensory fibres also innervate metabolic organs like liver and WAT, with an impact on the control of peripheral oscillators. These results suggest that this ion channel might constitute a temperature sensor in the retina which contributes to the precise control of the central clock, influencing the circadian characteristics of Tc. Finally, the presence of TRPM8 sensory fibres in metabolic peripheral tissues, like liver and WAT might constitute a bond between body Tc oscillations and the entrainment of peripheral clocks.

2 | RESULTS

2.1 | TRPM8 is expressed in the retina in cholinergic amacrine interneurons and in a subset of melanopsin retinal ganglion cells

TRPM8 is expressed in a subpopulation of primary sensory neurons and serves as the main sensor for cold temperature of the skin and mucosae. In addition, TRPM8 is also expressed in some non-neural cells and in neurons of the central nervous system, especially in thermoregulatory circuits.[25,26] Previously, we described the presence of TRPM8 immunolabelled fibres in the suprachiasmatic nucleus of the hypothalamus (SCN),[25] which constitutes the main pacemaker of circadian function. To get further insight into a possible role of TRPM8 in circadian regulation, we first searched for the expression of TRPM8 in the retina, because neurons in the SCN receive axonal projections principally from intrinsically photosensitive retinal ganglion cells (ipRGCs), responsible for synchronizing SCN neuron activity with light.[5]

We studied the presence of TRPM8 mRNA in the retina by conventional RT-PCR and RT-qPCR techniques. As shown in Figure 1A, we found detectable TRPM8 mRNA in this tissue (Ret), although at much lower levels than in trigeminal ganglia (Tg): 7.6 ± 2.3 vs 5060 ± 1208, as assessed by RT-qPCR; $p < 0.0001$, $n = 3$ mice. Thereafter, we used two reporter mouse lines (*Trpm8*$^{BAC\text{-}EYFP}$ and *Trpm8*^{EGFPf}) to characterize in more detail the TRPM8-positive neurons in the retina. In both mouse lines, we found GFP-labelled somas in the inner retina, specifically in the ganglion cell layer (GC) and in the inner nuclear layer (INL) (Figure 1B–J).

Because the photopigment melanopsin identifies ipRGCs,[6] we studied the possible colocalization of melanopsin and GFP. In the *Trpm8*$^{BAC\text{-}EYFP}$ line numerous GFP-positive cells were found in the inner retina, in the GC and INL (Figure 1C,D). Melanopsin labelled only ~1.5% of all GFP+ cells (1.4 ± 0.03%). However, about half of melanopsin-positive cells were also labelled with GFP (44.3 ± 2.15%).

Colocalization of melanopsin and GFP was also identified in the *Trpm8*^{EGFPf} transgenic line (Figure 1E,F). The lower GFP signal in these mice, and especially the low labelling of cell somas due to the farnesylated GFP,[27] prevented a precise quantification of the degree of colocalization.

Amacrine cells (ACs) form a highly diverse set of inhibitory interneurons in the inner retina, with their dendrites stratifying at different levels of the inner plexiform layer (IPL).[28] ChAT is a marker for starburst ACs.[29] ChAT-labelled somas were found in the INL and in the GC layer (i.e. displaced amacrine cells), with their dendrites stratifying into two well-defined bands in the IPL. They correspond to ON and OFF cells (Figure 1G,I). In the *Trpm8*$^{BAC\text{-}EYFP}$ line, nearly all ChAT-positive somas, in INL and GC layer, express GFP (95.3 ± 1.4% and 94.4 ± 4.4% respectively) (Figure 1G,H). Furthermore, both ChAT bands show a good colocalization with GFP. Of note, a fraction of GFP-positive cells in the INL did not colocalize with ChAT (~54%). This, and the presence of an additional non-ChAT GFP-labelled band in the most external part of the IPL suggest the presence of an additional population of non-ChAT ACs, expressing TRPM8 in this transgenic line. Similarly, almost all visualized GFP-positive neurons in the INL of *Trpm8*^{EGFPf} mice stained for ChAT, although, as mentioned above, quantification was not attempted due to the low levels of GFP (Figure 1I,J). In any case, both ChAT bands in this mouse line also showed co-labelling with GFP, supporting again the expression of TRPM8 in starburst ACs (Figure 1I).

We attempted to confirm the results obtained in these two reporter lines with immunocytochemistry, but none of the TRPM8 antibodies tested worked well in mice. However, in the rat we were able to detect TRPM8-immunoreactive cells in the GC layer and in some cells in the INL, presumably ACs (Figure 1K). Immunopositive fibres were observed running along the inner part of the GC layer (Figure 1K). Note that the immunolabelled signal is displaced by co-incubation with a blocking peptide (Figure 1L). Collectively, these results indicate that TRPM8 is expressed in cholinergic ACs and in a subset of ipRCG in both rodents.

2.2 | TRPM8-positive fibres from ipRGCs project to the SCN

We next investigated whether GFP-immunolabelled ipRGCs project to the SCN. To this end, we used the two different TRPM8 reporter mouse lines mentioned above

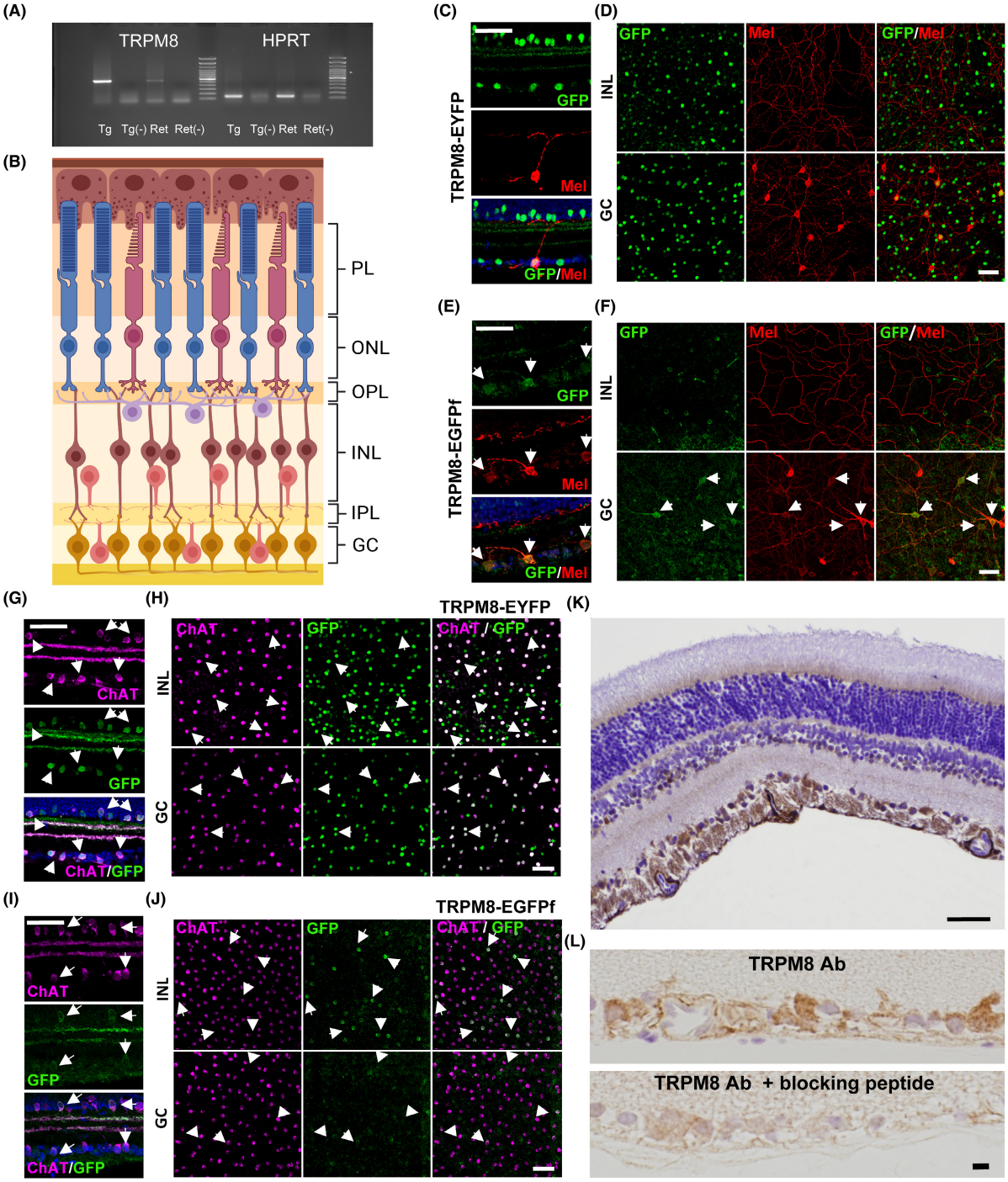

FIGURE 1

(*Trpm8*$^{BAC\text{-}EYFP}$ and *Trpm8*^{EGFPf}), injecting the fluorescent anterograde tracer cholera toxin subunit B (CTB-594) into both eyes. We found GFP-positive fibres travelling through the optic chiasm (Figure 2A) and innervating the SCN, principally its dorso-lateral part (Figure 2B). We did not observe labelled somas in this hypothalamic nucleus (Figure 2B). The intensity of labelling was dimmer in the *Trpm8*^{EGFPf} line, as described previously in sensory ganglia and other brain areas.[25] Interestingly, some of the CTB-594-positive fibres travelling through the optic chiasm co-express GFP (Figure 2A). Also, co-expression of both signals was found, especially in the lateral part of the SCN (Figure 2B,C). These data indicate the existence of ipRGCs expressing TRPM8 and projecting to the SCN.

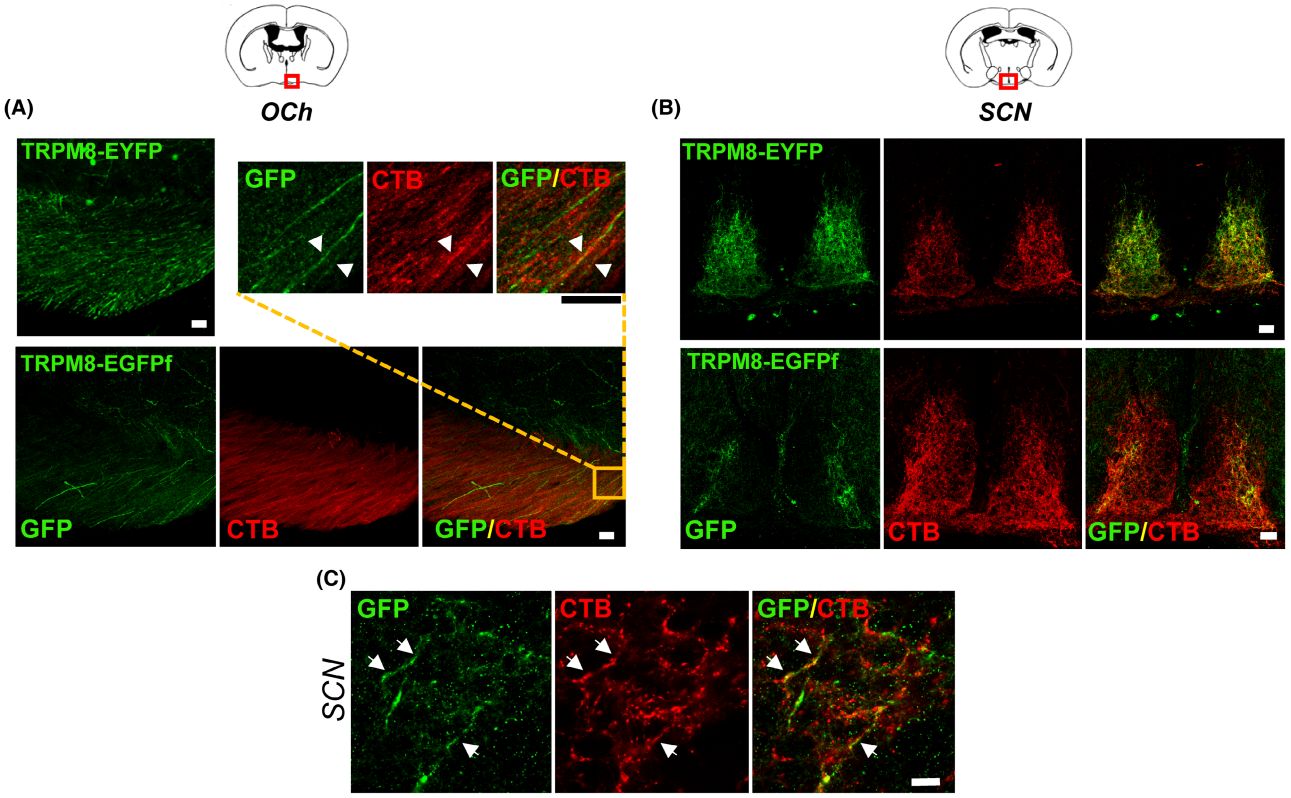

FIGURE 2 The suprachiasmatic nucleus (SCN) is innervated by TRPM8-positive axons originated in retinal ganglion neurons. The anterograde-labelling cholera toxin (CTB)-594 was injected into both eyes of *Trpm8*$^{BAC\text{-}EYFP}$ and *Trpm8*^{EGFPf} mice. Seventy-two hours after the injection, we studied the colocalization of GFP and CTB in the optic chiasm, OCh (A) and in the suprachiasmatic nucleus of the hypothalamus, SCN (B and C) by confocal microscopy. Notice the colocalization of fluorescent signals in some of the fibres (indicated by arrowheads). Experiments were performed in mice of 3–5 months of age (*Trpm8*$^{BAC\text{-}EYFP}$) and P15-21 (*Trpm8*^{EGFPf}). n = 3–4 mice/group. Both sexes were used indistinctively. Scale bars: (A) 25 μm. (B) 50 μm; (C) 10 μm.

2.3 | TRPM8-positive fibres innervate high blood flow ocular vascular structures and regulate eye temperature

The presence of TRPM8 inside the ocular globe is not restricted to retinal neurons. Using the *Trpm8*$^{BAC\text{-}EYFP}$ mouse line, we found TRPM8-immunolabelled fibres surrounding or travelling along choroidal vasculature and ciliary body capillaries (Figure 3A,B). The incubation without the primary antibody prevented the signal, as shown in the case of ciliary body (Figure S1A). This is an important finding because, the ciliary body, but mainly the choroid, constitutes the most important high-blood flow vascular structures in the eye and is known

FIGURE 1 A subset of melanopsin retinal ganglion cells (ipRGCs) and cholinergic amacrine cells express TRPM8. (A) TRPM8 RT-PCR in mouse trigeminal ganglion (Tg) and retina (Ret). Three micrograms of RNA were retrotranscribed and amplified by PCR. (−) Negative control without retrotranscriptase. HPRT was used as loading control. (B) Diagram of a cross section of mouse retina indicating the different layers. GC: Ganglionar cell layer; IPL: Inner plexiform layer; INL: Inner nuclear layer; OPL: Outer plexiform layer; ONL: Outer nuclear layer; PL: Photoreceptor layer. (C–F) Confocal images of GFP and/or melanopsin immunoreactivity in *Trpm8*$^{BAC\text{-}EYFP}$ (C and D) and *Trpm8*^{EGFPf} (E and F) mice. Tissue sections (C and E) and whole mount retinas (D and F) were used. (G–J) Confocal images of GFP and/or choline acetyl transferase (ChAT) immunolabelling in *Trpm8*$^{BAC\text{-}EYFP}$ (G and H) and *Trpm8*^{EGFPf} (I and J). Notice that G and I are tissue sections, and H and J are whole-mount retinas. (K and L) TRPM8-immunoreactive neurons and axons in paraffin-embedded rat retina sections. (L) Specificity control of the immunolabelled signal: Rat retinal sections were incubated with the TRPM8 antibody (above) or with the antibody in the presence of a blocking peptide (below). Experiments were performed in mice of 3–5 months of age (*Trpm8*$^{BAC\text{-}EYFP}$), postnatal day 15–21, P15-21 (*Trpm8*^{EGFPf}) and P21 (A). n = 3–4 mice/group. Rats were 3 months old (n = 3). Both sexes were used indistinctively. Scale bars: (C-J and K): 50 μm; (L): 10 μm.

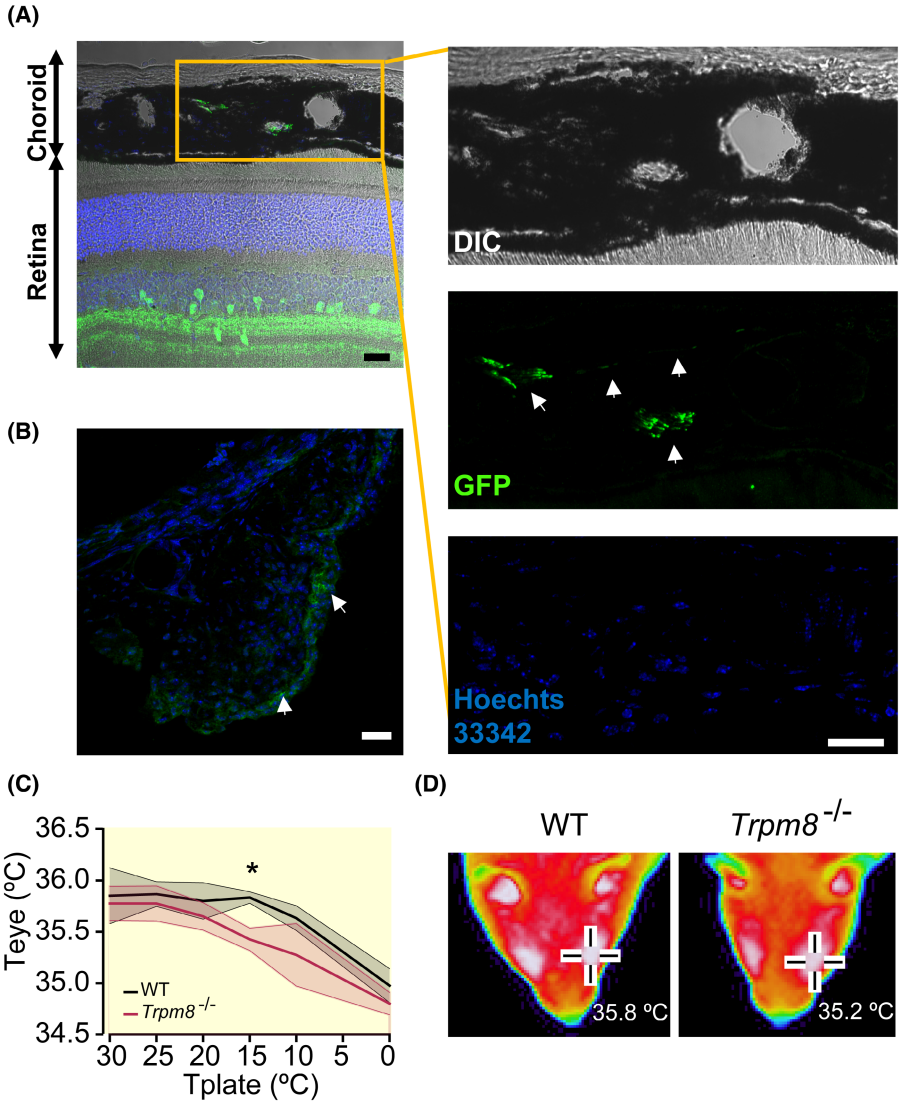

FIGURE 3 Choroid vasculature and ciliary body are innervated by TRPM8-positive fibres and TRPM8 regulates ocular temperature. Confocal images of GFP immunoreactive fibres travelling along and around choroidal vasculature (A) and in the ciliary body (B) of a *Trpm8*$^{BAC\text{-}EYFP}$ reporter mouse. Scale bar: 25 μm. DIC: Differential interference contrast. (C) Ocular temperature (Teye) was determined by infrared (IR) thermography in WT and *Trpm8*$^{-/-}$ mice exposed to different temperatures. Mice were placed on a steel platform and exposed to a cold ramp. The plate temperature (Tplate) was decreased linearly from 30 to 0°C (1°C/min). Teye was determined manually in each eye when the Tplate was 30, 25, 20, 15, 10 and 0°C, and the values analysed using the nonparametric Fisher's exact permutation test (MATLAB). *$p < 0.05$. (D) Representative infrared image of the eyes of a WT and a *Trpm8*$^{-/-}$ mouse when the steel surface was 15°C. Teye in the area marked by the cross was 35.8 and 35.2°C respectively. Experiments were performed in mice of 3–5 months of age (*Trpm8*$^{BAC\text{-}EYFP}$) and 4 months of age (WT and *Trpm8*$^{-/-}$). $n = 3$–6 mice/group. In (A and B) females and males were used indistinctively. In (C and D) mice were males and data were represented as mean ± SEM.

to regulate ocular and retinal temperature.[30] To study a possible role of TRPM8 in eye blood flow, we determined eye temperature (Teye) by infrared (IR) thermography in WT and *Trpm8*$^{-/-}$ mice exposed to different temperatures. Previous studies have shown that ocular haemodynamics can be estimated indirectly by measuring ocular surface temperature.[31,32] Mice were placed on a steel platform and exposed to a cold ramp. The plate temperature (Tplate) was decreased linearly from 30 to 0°C (1°C/min). In WT animals, Teye was maintained until Tplate reached 10°C, with a rapid decline thereafter. In animals lacking TRPM8, Teye started to decline at Tplate temperatures below 25°C and *Trpm8*$^{-/-}$ mice displayed a significantly lower Teye than WT littermates when Tplate was around 15°C (Figure 3C,D). This might suggest a function of TRPM8 and ambient temperature in regulating choroid and ciliary body blood flow and therefore involved in the control of internal ocular temperature.

2.4 | TRPM8 fine-tunes the expression of clock genes and neuropeptides in the SCN

The presence of TRPM8 in ipRGCs projecting to the SCN, and in ChAT amacrine interneurons regulating activity of retinal GCs, suggests a putative role of TRPM8 in central clock regulation. We therefore investigated several aspects of the circadian clockwork at the SCN in control and in *Trpm8*$^{-/-}$ mice. We determined the expression of the *Period2* gene (*Per*2), which is one of the essential components of core circadian clocks in the SCN[9] by 'in situ' hybridization. Our results in female mice confirmed previous data, showing a robust rhythmic oscillation of Per2 mRNA in the SCN of control mice in L/D conditions, with higher levels at ZT4 than at ZT16 (Figure 4A,B).[10,13,33] Interestingly, while the oscillation of Per2 mRNA was maintained in *Trpm8*$^{-/-}$ mice, we found in these animals a significant increase of ~40% in Per2 mRNA content in relation to WT littermates during the daytime (two-way ANOVA, genotype ($p = 0.001$) and light ($p = 0.001$). Post hoc analysis revealed significant differences between genotypes at

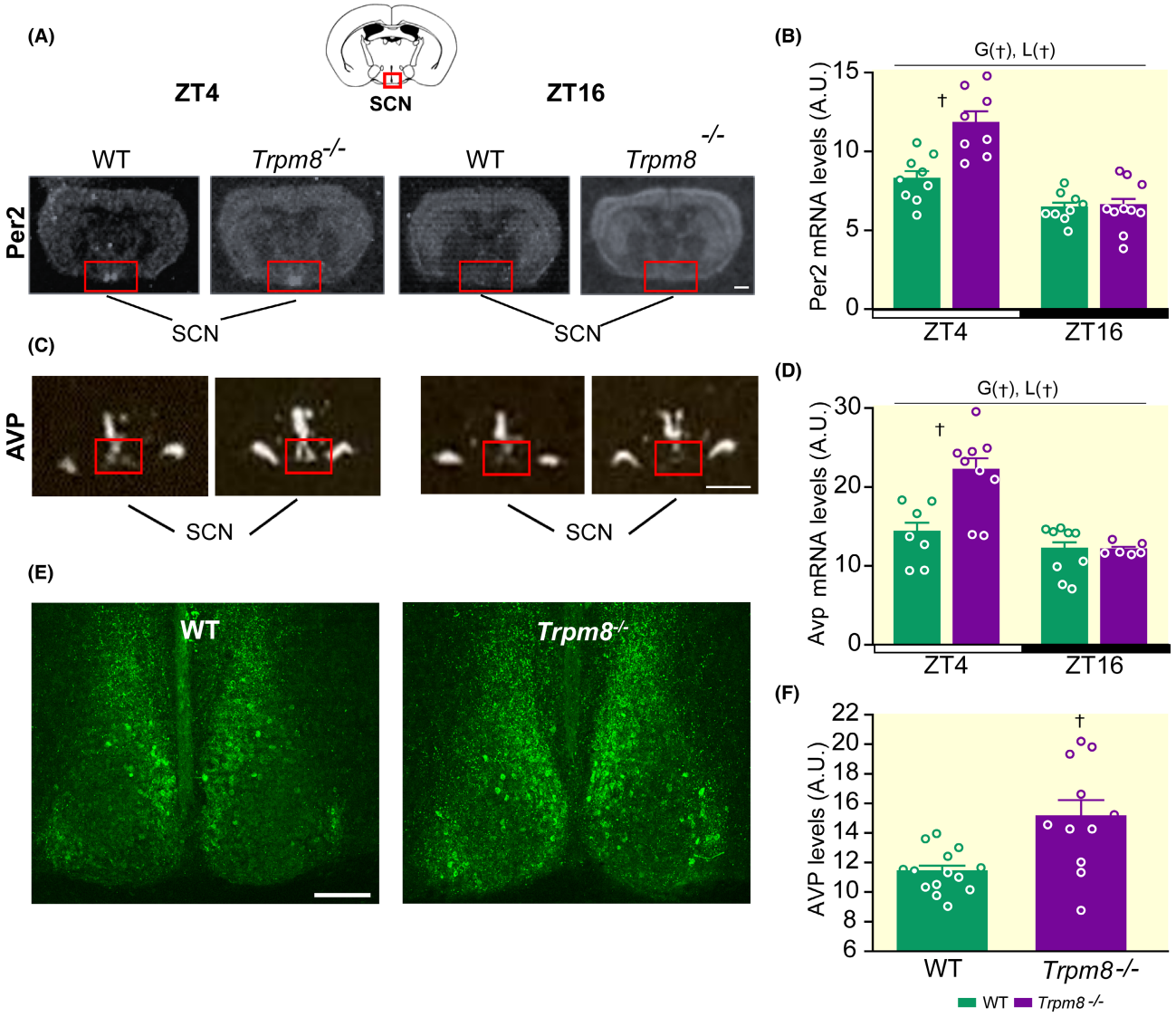

FIGURE 4 Per2 and AVP expression in the suprachiasmatic nucleus (SCN) are regulated by TRPM8. Per2 (A) and AVP (C) mRNA levels in the suprachiasmatic nucleus (SCN) of WT and *Trpm8*$^{-/-}$ mice at ZT4 and ZT16 detected by 'in situ' hybridization and quantification of their values (B and D). Scale bars in A and C: 2 mm. (E) AVP immunofluorescence in the SCN nucleus of WT and *Trpm8*$^{-/-}$ mice at ZT6. Scale bar: 100 μm. (F) Quantification of the AVP immunoreactive levels in the SCN. Experiments were performed in 6–14 female mice/group of 6–10 months of age. Data were represented as mean ± SEM. In B and D, statistical analysis was performed by two-way ANOVA, with genotype (G) and light (L) as factors. In (B): G ($p = 0.001$) and L ($p = 0.001$). Post hoc Bonferroni between gentypes in ZT4: $p < 0.01$. In (D) G ($p = 0.0066$) and L ($p = 0.0002$). Post hoc Bonferroni between genotypes in ZT4: $p < 0.01$). In (F) data were analysed by Student's *t* test ($p = 0.0079$). *$p < 0.05$; †$p < 0.01$.

ZT4, $p < 0.01$). Similar results were obtained in male mice (Figure S1B).

One of the most relevant clock-controlled genes (CCG) in the SCN is the gene coding for the neuropeptide AVP. AVP-expressing neurons in the SCN constitute the main output of this nucleus and are known to be involved in core temperature (Tc) circadian regulation.[11] We therefore studied Avp mRNA levels also at ZT4 and ZT16 by 'in situ' hybridization in the SCN of WT and TRPM8-deficient female mice. In control animals, we found a circadian oscillation of Avp mRNA, with higher levels at ZT4 than in ZT16, as already reported in the literature (Figure 4C,D).[10] *Trpm8*$^{-/-}$ mice also displayed greater *Avp* expression than control mice during the lights-on phase (~50% higher) but conserving the oscillation between day and night (Figure 4C,D) (two-way ANOVA, genotype ($p = 0.006$) and light ($p = 0.0002$). Post hoc analysis between genotypes at ZT4, $p < 0.01$).

AVP is also expressed in other hypothalamic nuclei but, in contrast to SCN, Avp mRNA in the paraventricular nucleus (PVN) did not exhibit either circadian rhythmicity or differences between the two genotypes (Figure S1C).

To confirm the effect of TRPM8 on AVP levels in the SCN, we examined AVP immunoreactive levels in both experimental groups by confocal microscopy. Animals were studied at ZT6, when vasopressin peptide levels are high.[34] As shown in Figure 4E,F, increased immunofluorescent levels were found in cell bodies and fibres in the SCN of TRPM8-deficient mice (Student's *t* test, $p = 0.0079$). In contrast, TRPM8 deletion did not affect AVP immunoreactivity in the PVN (Figure S1D).

Taken together, these results show that the absence of TRPM8 does not prevent the oscillatory expression of clock genes like *Per2* or neuropeptides like AVP in the SCN. However, our data suggest that TRPM8 is required to fine-tune their expression levels, implying that it might be involved in the regulation of circadian fluctuations of physiological parameters.

2.5 | TRPM8 regulates the amplitude and levels of body temperature oscillations

Because TRPM8 plays a critical role in the homeostatic aspects of thermoregulation,[24] we hypothesized that it might also be involved in the circadian regulation of body temperature (Tc). We therefore monitored Tc and motor activity in light/dark (L/D) and free-running conditions (dark/dark, D/D and light/light, L/L) in *Trpm8*$^{-/-}$ mice and littermate controls.

Male animals were housed at 21°C and maintained in L/D for 7 days and then released in D/D for 34 days. TRPM8 deletion in L/D conditions induced a drop in Tc levels, especially during the daytime (Figure 5A). Interestingly, while WT mice in constant darkness displayed a progressive reduction in mean Tc values (Figure 5B and Table 1), TRPM8-deficient mice maintained the same low mean Tc levels in L/D and D/D conditions (Figure 5C and Table 1). In addition, TRPM8 deletion induced a significant reduction in minimum Tc levels (two-Way ANOVA, genotype: $p = 0.0063$) and an increase of ~0.5°C in the amplitude of Tc oscillations (two-way ANOVA, genotype: $p = 0.0082$) (Figure 5E,F and Table 1).

We did not observe significant differences in rhythmic parameters between both genotypes. Exposure to D/D produced a comparable advancement in the time of daily rise in Tc (temperature rising phase) in *Trpm8*$^{-/-}$ and WT littermates (Figure S2A,B and Table 1).

The decreased levels of Tc displayed in the absence of TRPM8 were not the result of lower motor activity, as demonstrated by measuring this parameter with the same telemetric devices employed to record Tc. Although both experimental groups displayed a progressive drop of motor activity during long-term D/D conditions, WT mice experienced a greater reduction (Figure S2C–F and Table 2).

To get further insight into the role of TRPM8 in Tc circadian regulation, mice were left in constant dim light (80–90 lux, L/L) for 21 days. Tc in TRPM8-deficient animals showed a greater phase delay, compared to WT animals, and a very unstable rhythmicity, as it is shown in Figure 5G. Indeed, after 7 days in L/L *Trpm8*$^{-/-}$ mice already exhibited a significant greater delay in the rising phase of Tc in relation to control mice (CT: 19.19 ± 0.30 vs 17.17 ± 0.44, $p = 0.005$) (Figure 5H,I). Furthermore, 50% of *Trpm8*$^{-/-}$ mice lost circadian rhythm of Tc after 15 days in LL, while all WT littermates still displayed robust Tc circadian oscillations.

Additional experiments were performed on a cohort of adult female mice also housed at 21°C. WT and *Trpm8*$^{-/-}$ animals were studied in L/D conditions for 5 days (Figure 5J) and then released in D/D for another 5 days (Figure 5K). TRPM8 deletion induced higher maximum Tc levels (two-way ANOVA, genotype $p = 0.03$), a tendency to lower minimum Tc values (genotype $p = 0.07$) and a greater amplitude of Tc oscillations than controls (an increase of ~0.69°C) (two-way ANOVA, genotype: $p = 0.024$) (Figure 5J–L, Figure S2G,H and Table 3). *Trpm8*$^{-/-}$ mice in D/D showed a tendency to display an earlier daily rise in Tc than WT ($p = 0.08$) (Figure 5K). When female mice were left in L/L for 5 days, *Trpm8*$^{-/-}$ animals showed a significant reduction of body temperature, determined as rectal temperature in relation to controls (Figure S2I).

Mice were also studied at 29°C, the lowest Ta of their thermoneutral zone. Male animals were maintained in L/D for 7 days and released thereafter in constant darkness (D/D) for another 7 days. Interestingly, while in

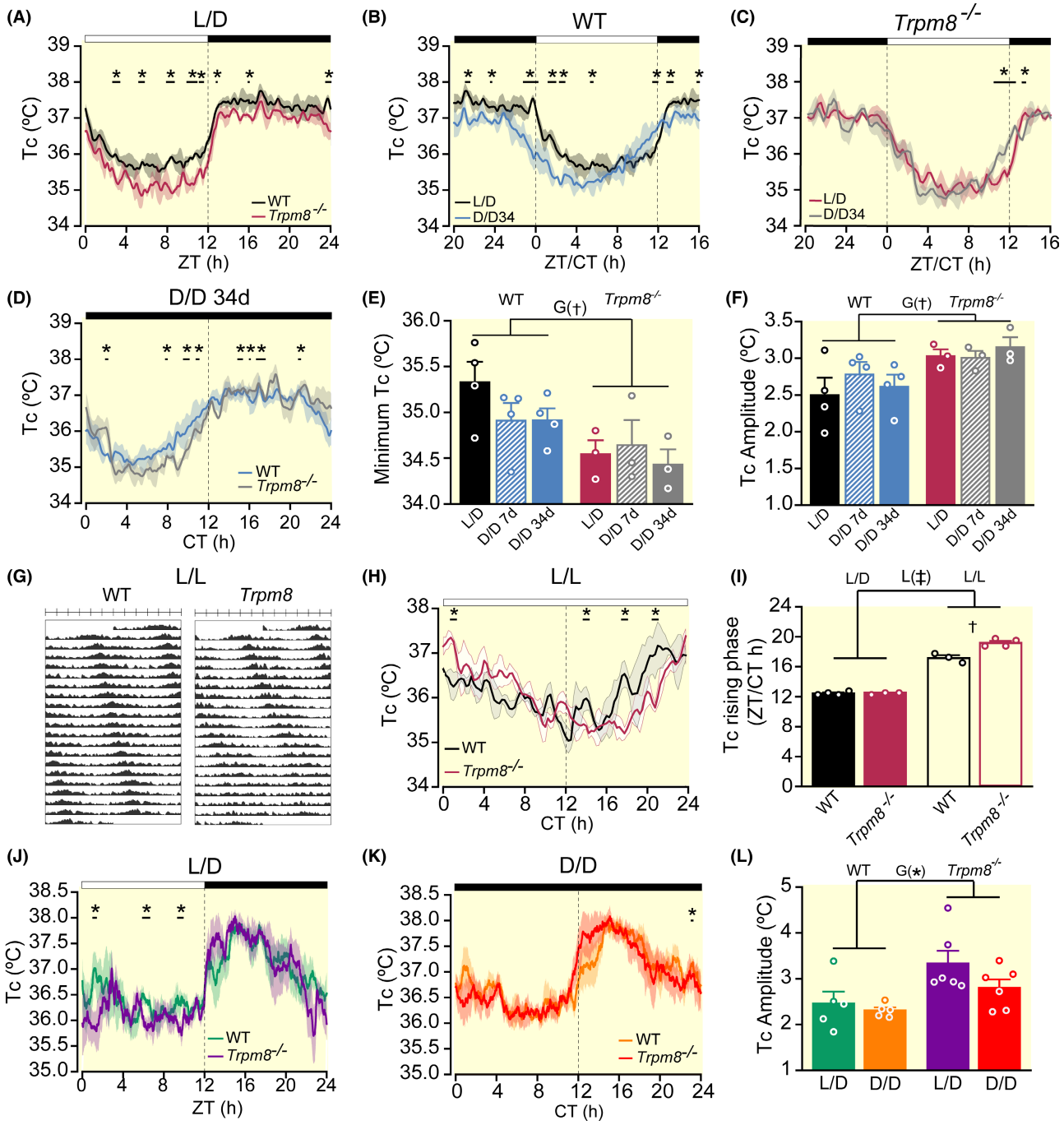

FIGURE 5 Circadian Tc oscillations are fine-tuned by TRPM8. Continuous telemetric recordings of Tc in mice housed at 21°C. WT and *Trpm8*$^{-/-}$ male mice were exposed to light–dark conditions 12/12 (L/D) for 7 days (A) and then released in constant darkness (D/D) for 34 days (B-F), or in constant light (L/L) for 21 days (G–I). The graphs represent daily average of the Tc values recorded during the last 3 days of each condition and statistical analysis of Tc was performed with the non-parametric Fisher's exact permutation test (MATLAB). (A) Tc values of WT and *Trpm8*$^{-/-}$ mice housed in L/D conditions. Representation of Tc values in WT (B) and *Trpm8*$^{-/-}$ (C) mice in L/D and after 34 days in D/D. (D) Tc in WT and *Trpm8*$^{-/-}$ mice after 34 days in D/D. Minimum levels (E) and amplitude (F) of Tc oscillations in WT and *Trpm8*$^{-/-}$ housed in L/D and in D/D for 7 and 34 days. Tc minimum values (two-way ANOVA, genotype: G ($p = 0.0063$). Tc amplitude (two-way ANOVA, genotype, G: $p = 0.0082$). (G) Double temperogram of WT and *Trpm8*$^{-/-}$ mice exposed to L/L for 21 days. (H) Tc values of these mice after 7 days in L/L. (I) Time (ZT/CT) of daily rise in Tc (Tc rising phase) in WT and *Trpm8*$^{-/-}$ mice after 7 days in L/L (two-way ANOVA, lighting conditions, L: $p < 0.001$; Post hoc Bonferroni between genotypes in L/L: $p = 0.005$). (J–L) WT and *Trpm8*$^{-/-}$ female mice were housed in light–dark conditions 12/12 (L/D) for 5 days and then released in constant darkness (D/D) for 5 days. The graphs represent daily average of the Tc values recorded during the last 3 days of each condition. Tc values in L/D conditions (J) and in D/D conditions (K). (L) Tc amplitude in WT and *Trpm8*$^{-/-}$ mice in L/D and D/D (two-way ANOVA, genotype, G: $p = 0.024$). Experiments were performed in 3–4 male mice/group of 8–9 months of age (A–I) and in 5–7 female mice/group of 4–5 months of age (J-L). Data were represented as mean ± SEM. *$p < 0.05$; †$p < 0.01$; ‡$p < 0.001$.

TABLE 1 Tc parameters of male mice exposed to light–dark 12/12 (L/D) for 7 days and then released in constant darkness (D/D)

	L/D		D/D 7 days		D/D 34 days		
Tc	**WT**	***Trpm8*$^{-/-}$**	**WT**	***Trpm8*$^{-/-}$**	**WT**	***Trpm8*$^{-/-}$**	**Ta**
Maximum (°C)	37.36 ± 0.08	37.43 ± 0.06	37.60 ± 0.12	37.51 ± 0.06			29°C
	37.83 ± 0.14	37.58 ± 0.15	37.76 ± 0.16	37.43 ± 0.17	37.54 ± 0.07	37.58 ± 0.22	21°C
Minimum (°C)	35.54 ± 0.08	35.62 ± 0.05	35.33 ± 0.10	34.91 ± 0.07 $p = 0.001$ (vs WT DD7)			29°C
	35.33 ± 0.26	34.55 ± 0.19 G ($p = 0.0063$)	34.91 ± 0.22	34.65 ± 0.34 G ($p = 0.0063$)	34.92 ± 0.15	34.43 ± 0.21 G ($p = 0.0063$)	21°C
Mean (°C)	36.39 ± 0.05	36.43 ± 0.05	36.43 ± 0.12	36.21 ± 0.04			29°C
	36.63 ± 0.15	36.20 ± 0.12 G ($p = 0.0013$)	36.43 ± 0.10	36.09 ± 0.07 G ($p = 0.0013$)	36.28 ± 0.04 $p = 0.049$ (vs WT LD)	36.18 ± 0.13 G ($p = 0.0013$)	21°C
Amplitude (°C)	1.82 ± 0.09	1.8 ± 0.07	2.27 ± 0.08	2.60 ± 0.09 $p = 0.01$ (vs WT DD7)			29°C
	2.49 ± 0.27	3.03 ± 0.11 G ($p = 0.0082$)	2.78 ± 0.19	3.01 ± 0.11 G ($p = 0.0082$)	2.61 ± 0.18	3.15 ± 0.16 G ($p = 0.0082$)	21°C
Rising phase (ZT/CT h)	12.07 ± 0.05	11.91 ± 0.17	11.45 ± 0.09 L ($p = 0.002$)	11.10 ± 0.17 L ($p = 0.002$)			29°C
	12.44 ± 0.14	12.42 ± 0.10	13.00 ± 0.31	12.92 ± 0.1	11.50 ± 1.61 $p = 0.03$ (vs WT LD)	11.25 ± 0.47 $p = 0.04$ (vs KO LD)	21°C

Note: Mice were studied at 2 ambient temperatures (Ta): 29 and 21°C. Data in D/D after 7 days (D/D 7 days) and after 34 days (D/D for 34 days) are shown. Statistical significance was analysed by two-way ANOVA, with genotype (G) and lighting condition (L) as factors. Bonferroni test was used as post hoc analysis. Data are represented as mean ± SEM. Mice were males of 4–5 months of age in the experiments at 29°C ($n = 11$–13 mice/group) and of 8–9 months in the experiments at 21°C ($n = 3$–4 mice/group). [Correction added on December 2, 2022. In the first column, Mean (h) has been corrected to Mean (°C)]

TABLE 2 Motor activity of male mice exposed to light–dark 12/12 (LD) for 7 days and then released in constant darkness (D/D)

Activity	LD		DD 7 days		DD 34 days		Ta
	WT	*Trpm8*$^{-/-}$	WT	*Trpm8*$^{-/-}$	WT	*Trpm8*$^{-/-}$	
Diurnal/ Subjective day accumulated motor activity (arbitrary units)	647.8 ± 347.1	1031.5 ± 413.8	934.2 ± 574.6	1241.4 ± 670.0			29°C
	5401.8 ± 574.3	5112.4 ± 975.1	6148.5 ± 513.9	7193.5 ± 1273.4	5211.2 ± 667.6	6300.0 ± 698.5	21°C
Nocturnal/subjective night accumulated motor activity (arbitrary units)	7183.9 ± 1652.0	7025.3 ± 1766.8	6858.1 ± 1938.1	7183.7 ± 1883.8			29°C
	14536.1 ± 1275.4	17234.0 ± 679.2	11855.6 ± 531.2	13416.8 ± 2720.8	8714.6 ± 733.7	12115.0 ± 703.1 $p = 0.015$ (vs WT DD34)	21°C
Total accumulated motor activity (arbitrary units)	7831.8 ± 1999.1	8056.9 ± 2180.7	7792.3 ± 2512.8	8425.1 ± 2553.8			29°C
	19937.9 ± 1772.7	22346.5 ± 1178.1	18004.2 ± 547.6	20610.4 ± 2518.4	13925.9 ± 540.4	18415.08 ± 1307.4 $p = 0.018$ (vs WT DD34)	21°C

Note: Mice were studied at 2 ambient temperatures (Ta), 29 and 21°C. Data in D/D after 7 days (D/D 7 days) and after 34 days (D/D for 34 days) are shown. Statistical significance was analysed by two-way ANOVA, with genotype (G) and lighting condition (L) as factors. Bonferroni test was used as post hoc analysis. Data are represented as mean ± SEM. Mice were males of 4–5 months of age in the experiments at 29°C (n = 11–13 mice/group) and of 8–9 months in the experiments at 21°C (n = 3–4 mice/group).

L/D conditions no significant differences were observed in Tc between both experimental groups (Figure 6A and Table 1), in D/D TRPM8-deficient mice displayed significantly lower minimum Tc values (Figure 6B–D and Table 1). Analysis of Tc oscillations revealed a greater amplitude of circadian fluctuations of Tc in *Trpm8*$^{-/-}$ vs WT mice in DD conditions (Student's t test, $p = 0.01$) (Figure 6E). No significant differences in rhythmic parameters were found between both genotypes, showing similar values of time of Tc rising phase in D/D (Table 1). The decreased levels of Tc displayed in the absence of TRPM8 in the subjective day were not the result of lower motor activity (Figure 6F and Table 2).

Collectively, our data suggest that TRPM8 plays a role in the physiology of the central oscillator controlling Tc.

2.6 | TRPM8 regulates clockwork in liver and fat

Because oscillation of body temperature appears to be a major factor regulating peripheral clocks,[20] and our results indicate a role of TRPM8 in the circadian fluctuations of Tc, we next studied the possible impact of this ion channel on peripheral clockwork. We focused on liver and white adipose tissue (WAT) because they are two well-known metabolic oscillators.[35] We first searched for the presence of this ion channel in these tissues. With the *Trpm8*$^{BAC\text{-}EYFP}$ reporter mouse line, we identified a rich innervation of GFP-immunolabelled fibres in both organs. We did not observe TRPM8-positive cells. In the liver, GFP-fibres innervate principally the hilum area, especially surrounding the portal vein and hepatic vessels (Figure 7A,B). In the case of the gonadal WAT, we also found nervous trunks with TRPM8-positive sensory fibres (Figure 7C), especially travelling along associated vascular vessels (Figure 7D). These findings suggest that TRPM8 sensory innervation of liver and WAT might constitute a bond between body Tc oscillations and the entrainment of peripheral clocks. We therefore determined in both tissues the expression levels of *Per2* mRNA at ZT4 and ZT16 in WT and *Trpm8*$^{-/-}$ mice by conventional RT-PCR and RT-qPCR, with similar results. RT-qPCR results of female mice were represented in Figure 7E,F. Liver and WAT *Per2* mRNA levels in wild-type animals displayed a very marked oscillation, with low levels during the lights-on phase and high levels during the night, as already reported by others.[13,36] In contrast, TRPM8-deletion induced a marked dysregulation in the expression of this clock gene in both tissues. The analysis of *Per2* mRNA levels in the liver of male mice also revealed significant differences between both experimental groups, especially during the light phase (Figure S2J). All this indicates a clear function of TRPM8 also in peripheral oscillators.

TABLE 3 Tc parameters of female mice housed at 21°C and exposed to light–dark 12/12 (L/D) for 5 days and then released in constant darkness (D/D) for 5 days

	L/D		D/D 5 days	
Tc	**WT**	***Trpm8*$^{-/-}$**	**WT**	***Trpm8*$^{-/-}$**
Maximum (°C)	38.03 + 0.14	38.29 + 0.16 G ($p = 0.03$)	38.17 + 0.21	38.40 + 0.09 G ($p = 0.03$)
Minimum (°C)	35.57 + 0.46	34.96 + 0.47	35.86 + 0.16	35.60 + 0.33
Mean (°C)	36.75 + 0.23	36.65 + 0.17	37.01 + 0.18	36.86 + 0.20
Amplitude (°C)	2.46 + 0.41	3.33 + 0.48 G ($p = 0.024$)	2.31 + 0.1	2.80 + 0.32 G ($p = 0.024$)
Rising phase (ZT/CT h)	13.00 + 0.89	12.63 + 0.70	13.45 + 0.76	11.96 + 1.08

Note: Statistical significance was analysed by two-way ANOVA, with genotype (G) and lighting condition (L) as factors. Data are represented as mean ± SEM. Mice were females of 4–5 months of age ($n = 5$–7 mice/group). [Correction added on December 2, 2022. In the first column, Mean (h) has been corrected to Mean (°C)]

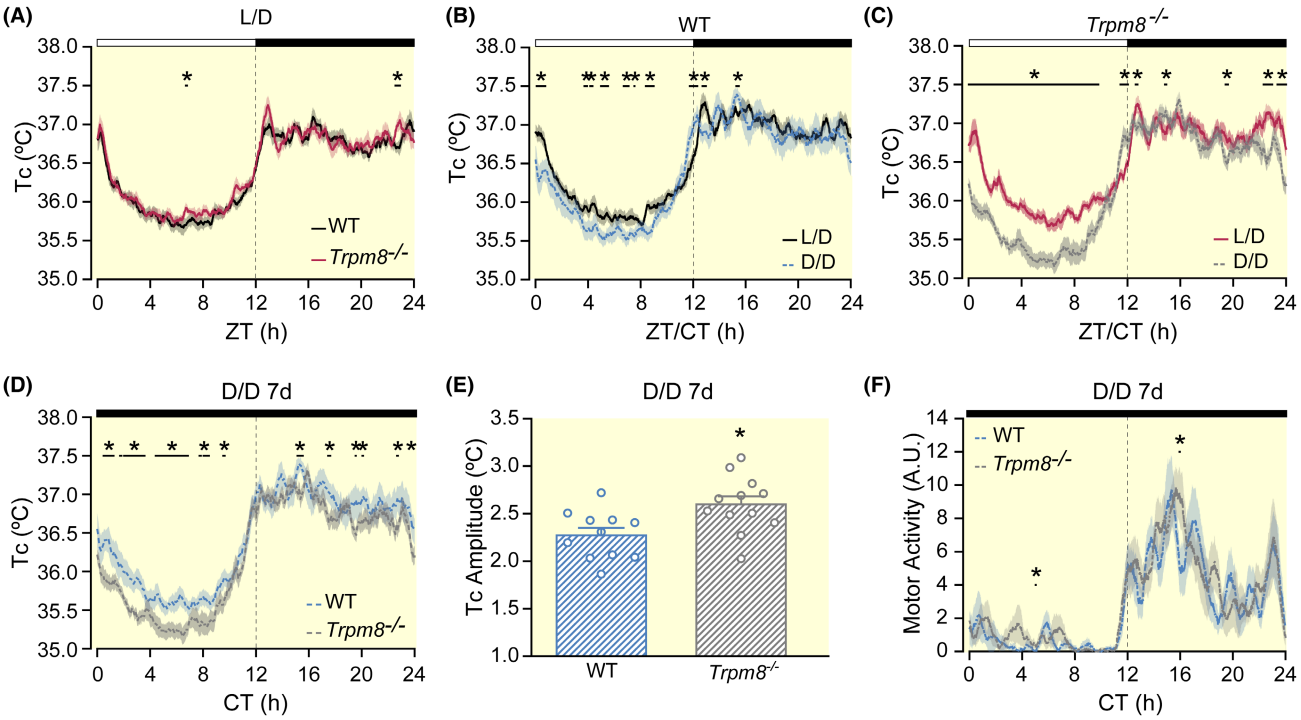

FIGURE 6 TRPM8 regulates circadian oscillations of Tc also at thermoneutrality. Continuous telemetric recordings of Tc (A–E) and motor activity (F) in male mice housed at an ambient temperature (Ta) of 29°C and exposed to light–dark conditions 12/12 (L/D) for 7 days and then released in constant darkness (D/D) for another 7 days. The graphs represent daily average of the Tc values recorded during the last 3 days of each condition and statistical analysis of Tc and motor activity was performed with the nonparametric Fisher's exact permutation test (MATLAB). (A) Tc values in WT and *Trpm8*$^{-/-}$ mice housed in L/D conditions. Representation of Tc values in WT (B) and *Trpm8*$^{-/-}$ (C) mice in L/D and after 7 days in D/D. (D) Tc in WT and *Trpm8*$^{-/-}$ mice after 7 days in D/D. (E) Amplitude of Tc oscillations in WT and *Trpm8*$^{-/-}$ mice housed in D/D for 7 days. Statistical analysis of Tc amplitude was performed with t-test ($p = 0.01$). (F) Motor activity of WT and *Trpm8*$^{-/-}$ mice housed in D/D for 7 days. Experiments were performed in 11–13 male mice of 4–5 months of age. Data were represented as mean ± SEM. *$p < 0.05$.

3 | DISCUSSION

Biological thermal detection is primarily based on the physiology of a subfamily of ion channels, highly conserved in evolution, called thermosensitive Transient Receptor Potential (TRP) channels. In mammals, the principal sensor for mild cold temperatures is TRPM8,[22,23,37,38] a non-selective cation channel that is expressed in peripheral sensory neurons innervating the skin and mucosae,[26,27,39] but also in internal organs including the brain.[25] Here, we show TRPM8 expression in a subset of ipRGCs neurons in retina which innervates the SCN. Furthermore, we found that TRPM8 is also expressed in cholinergic ACs, characterized by the release

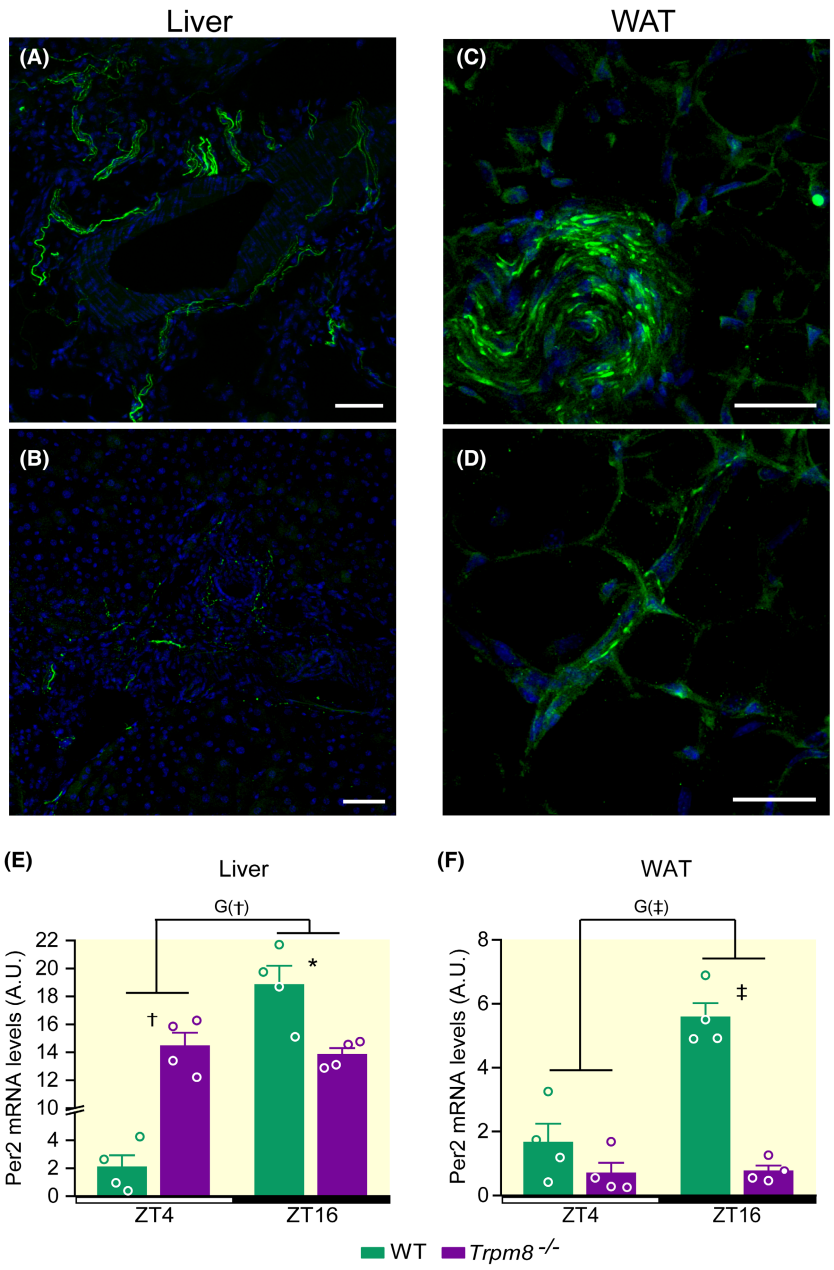

FIGURE 7 Liver and gonadal WAT are innervated by TRPM8-positive sensory fibre and TRPM8 regulates peripheral clocks in these tissues. (A–D) Confocal images of GFP in *Trpm8*$^{BAC\text{-}EYFP}$ mice corresponding to liver (A and B) and WAT (C and D). In the liver, many immunolabelled fibres were found in the hilum (A). Deeper areas of the organ displayed less number of positive fibres (B). GFP-labelled fibres were mainly associated to hepatic portal vessels. In gonadal WAT, we observed nerve trunks with immunolabelled fibres (C), and also fibres associated to vessels (D). Scale bars: (A and B): 50 μm; (C and D): 25 μm. Expression levels of Per2 mRNA in liver (E) and gonadal WAT (F) in WT and *Trpm8*$^{-/-}$ mice at ZT4 and ZT16 by RT-qPCR. Experiments were performed in four female mice/group of 9 months of age. Data were represented as mean ± SEM. Statistical significance was determined by two-way ANOVA, with genotype (G) and Light (L) as factors. Per 2 liver (G: $p = 0.0028$. Post hoc Bonferroni between genotypes in ZT4, $p < 0.01$; at ZT16, $p < 0.05$). Per2 gonadal WAT (G: $p < 0.001$. Post hoc Bonferroni between genotypes in ZT16, $p < 0.001$). *$p < 0.05$; $^{\dagger}p < 0.01$; $^{\ddagger}p < 0.001$.

of two neurotransmitters, GABA and acetylcholine.[29,40] The TRPM8-positive amacrine cells are probably ON and OFF type, considering the colocalization of GFP and ChAT in both labelled bands in the IPL.

Our demonstration of TRPM8 expression in rodent retinal neurons begs the question of temperature homeostasis in the retina. The choroid vasculature, and to a lesser extent the ciliary body, are known to play a major role in maintaining the intraocular thermal environment.[30,41] Specifically, the choroid would act as a thermostat thanks to the innervation by sensory trigeminal nerve fibres, which express CGRP and substance P, vasoactive compounds. In addition, sympathetic and parasympathetic fibres regulate choroidal blood flow.[30] Our results, showing innervation of choroid vasculature by sensory TRPM8-positive fibres, identifies this ion channel as a potential molecular cold sensor in these vessels and therefore as an important player in ocular temperature regulation. Indeed, our results show that *Trpm8*$^{-/-}$ mice exhibit a higher drop in Teye than controls when exposed to mild cold. Consistent with our findings, a previous study revealed that temperature in the vitreous chamber above or below 34°C induces an increase in choroidal blood flow (ChBF), and only when intraocular temperature falls below 16°C, the ChBF decreases.[42] We therefore propose that mild drops of temperature inside the eye would be detected by TRPM8 channels in the sensory trigeminal fibres innervating choroidal vasculature, which will produce an increase in ChBF to maintain the intraocular temperature. Whether vasodilation is mediated by

the release of CGRP or Substance P, or is due to a central loop, merits further investigation. Of note, it was previously demonstrated that a subset of trigeminal fibres in the cornea expressing low levels of TRPM8 also contains CGRP.[43]

More work is also needed to dissect the functional role of TRPM8 in starburst amacrine interneurons and ipRGCs in the retina. In that sense, it is worth noting that rhodopsin, a light-sensitive GPCR, plays a crucial function in thermotactic behaviours in fruit flies,[44] suggesting that an accessory factor might interact with rhodopsin and accelerate its intrinsic thermal activity. A similar mechanism could be operational in mice, modulating temperature sensitivity of melanopsin/TRPM8 expressing RGCs. Future experiments will examine the influence of temperature and TRPM8 agonists on the activity of ipRGCs in the retina.

Tracing TRPM8-positive axons from ipRGCs we found that they project to the SCN, mainly to the latero-dorsal part, characterized by a high density of arginine vasopressin (AVP) -producing neurons, and for high levels of *Per2*, a central gene in circadian rhythmicity.[45–47] *Avp* constitutes a clock-controlled gene (CGG) in mammalian SCN, and neurons containing this neuropeptide exert control over numerous circadian functions, including Tc cycle regulation.[11] In rodents, AVP transcription and secretion from the SCN has a diurnal pattern, reaching its peak during the light phase, and a trough at night-time.[48,49] This pattern of expression is similar to that observed for *Per2* in this nucleus.[10,33,50] Considering that *AVP* and *Per2* are under the control of *Clock*,[10] it is likely that these two genes share the same overexpressing mechanism in *Trpm8*$^{-/-}$ mice. It is important to underline that in the absence of TRPM8 *AVP* and *Per2* maintained their normal daily expression pattern, but their levels in ZT4 were higher than those in WT littermates. This agrees with the general concept of temperature compensation described for SCN neurons: a relative constancy of the period of oscillations but with differences in the levels or amplitudes of the fluctuations.[18]

SCN efferents innervate different brain regions, including the preoptic area (POA) of the hypothalamus, the main thermoregulatory centre in the brain. Specifically, the median preoptic nucleus (MnPO) in the POA receives direct projections from SCN vasopressinergic neurons and these efferent AVP axons would be part of a neuronal circuit involved in the regulation of Tc circadian oscillation.[11] Our results showing that TRPM8 regulates SCN AVP levels made us hypothesize a function of this channel in the circadian regulation of Tc. We therefore recorded continuously Tc and locomotor activity in wildtype and *Trpm8*$^{-/-}$ mice in driven (L/D) and free running conditions (D/D and L/L) and found that deletion of TRPM8 increases the amplitude of Tc oscillations. Importantly, no differences were detected in motor activity between *Trpm8*$^{-/-}$ mice and control animals, as recently shown.[51] This suggests that the increased amplitude of Tc rhythms observed in the absence of TRPM8 is independent of motor activity.

Interestingly, although in constant darkness, we were not able to find significant differences in the rhythm of the Tc cycle of *Trpm8*$^{-/-}$ mice versus WT, notable alterations emerged when these animals were housed under continuous dim light conditions (L/L). Thus, TRPM8-deficiency induced a greater delay in the daily Tc rising phase and a very unstable rhythmicity. Collectively, our findings suggest that TRPM8 regulates the physiology of the central oscillator controlling Tc.

Finally, the SCN hierarchically organizes and synchronizes peripheral clocks to advantageously display their function at the right time of day and, therefore, optimize resources. In addition to the classical routes by which SCN entrain peripheral clocks through the neuroendocrine system,[52] some authors have proposed that body temperature oscillations might work as a universal internal signal that participates in the entrainment of peripheral clocks.[20,53] Because the absence of TRPM8 induces Tc oscillations of greater amplitude, we hypothesized that this effect could act as an entrainer of peripheral oscillators. To assess this proposal, we chose liver and WAT due to their importance in metabolism and their well-studied circadian activity.[35] We have shown that both tissues are richly innervated by TRPM8 sensory fibres, especially associated to blood vessels. The innervation of the portal vein by TRPM8 sensory fibres has already been reported by McCoy et al.[54] and by our group.[26] On the other hand, modest TRPM8 expression, determined by RT-PCR, has been also described in human liver,[55] but these findings await confirmation by different techniques with cellular resolution. In relation to WAT, other authors have reported the presence of TRPM8 in a mouse WAT cell line and in cultured human and mouse adipocytes.[56–58] Nevertheless, in our hands, we were not able to find credible immunolabelling in hepatocytes or adipocytes. In any case, the presence of TRPM8 sensory fibres in liver and WAT in association with vascular structures suggests a function of these channels as thermal sensors in perivascular areas with an impact on the physiology of both organs. Indeed, the absence of TRPM8 greatly impaired clockwork in these two metabolic tissues, which highlights TRPM8 sensory information as a major factor regulating liver and WAT circadian cycles. Our findings, coupled with the application of novel molecular tools to define and manipulate sensory innervation in an organ-specific manner,[59] will shed light on the relevance and the molecular signals of the communication between dorsal root ganglia (DRG) neurons and peripheral organs, like WAT and liver.

Limitations of the study: As we used a global TRPM8-KO mouse in this study, we cannot definitively

demonstrate that TRPM8 fibres projecting to the SCN from the retina are the only regulators of the central clockwork. TRPM8 peripheral sensors, mainly in skin, might also play an indirect role mediating this effect, especially through the control of body temperature. While our study focused on the role of the genuine cold sensor TRPM8, it is well known that different potassium channels also play critical roles in modulating the thermosensitivity of neurons in the central and peripheral nervous system. Thus, their possible role in circadian thermoregulation merits further inquiries.[60,61]

In conclusion, TRPM8 is expressed in a subset of retinal interneurons and output neurons projecting to the SCN, the master clock. The activity of TRPM8 fine tunes clockwork and neuropeptide levels in this hypothalamic nucleus, contributing to the regulation of the circadian oscillation of Tc. These Tc fluctuations will be detected by TRPM8 in peripheral organs, including liver and WAT, serving as entrainers for peripheral oscillators in these metabolic tissues (Figure 8). Although further studies are necessary to delineate the precise role of TRPM8 in the retina, SCN and in the periphery, including fat tissue and liver, the present work provides strong evidence for TRPM8 serving as a link between temperature and central and peripheral clocks, regulating the circadian oscillations of body temperature.

4 | MATERIALS AND METHODS

4.1 | Animal models

Trpm8$^{-/-}$ mice were generated in the laboratory of David Julius and obtained from The Jackson Laboratories (stock #008198). Mice were maintained in heterozygosity by crossing to C57B6/J mice from Harlan Laboratories. Littermate wildtype mice were used as controls in all experiments (wildtype, WT).

Two different transgenic mouse lines were used as TRPM8 reporters: (a) A BAC containing the full TRPM8 sequence was engineered to generate by homologous recombination a mouse expressing the enhanced yellow fluorescent protein (EYFP) under the TRPM8 promoter (*Trpm8*$^{BAC\text{-}EYFP}$).[61] (b) Mice engineered to express the farnesylated enhanced green fluorescent protein (EGFPf) from the TRPM8 locus (*Trpm8*^{EGFPf}; B6;129S1[FVB]-*Trpm8*^{tm1Apat}/J) were obtained from Ardem Patapoutian (Scripps Research Institute). The targeted insertion of

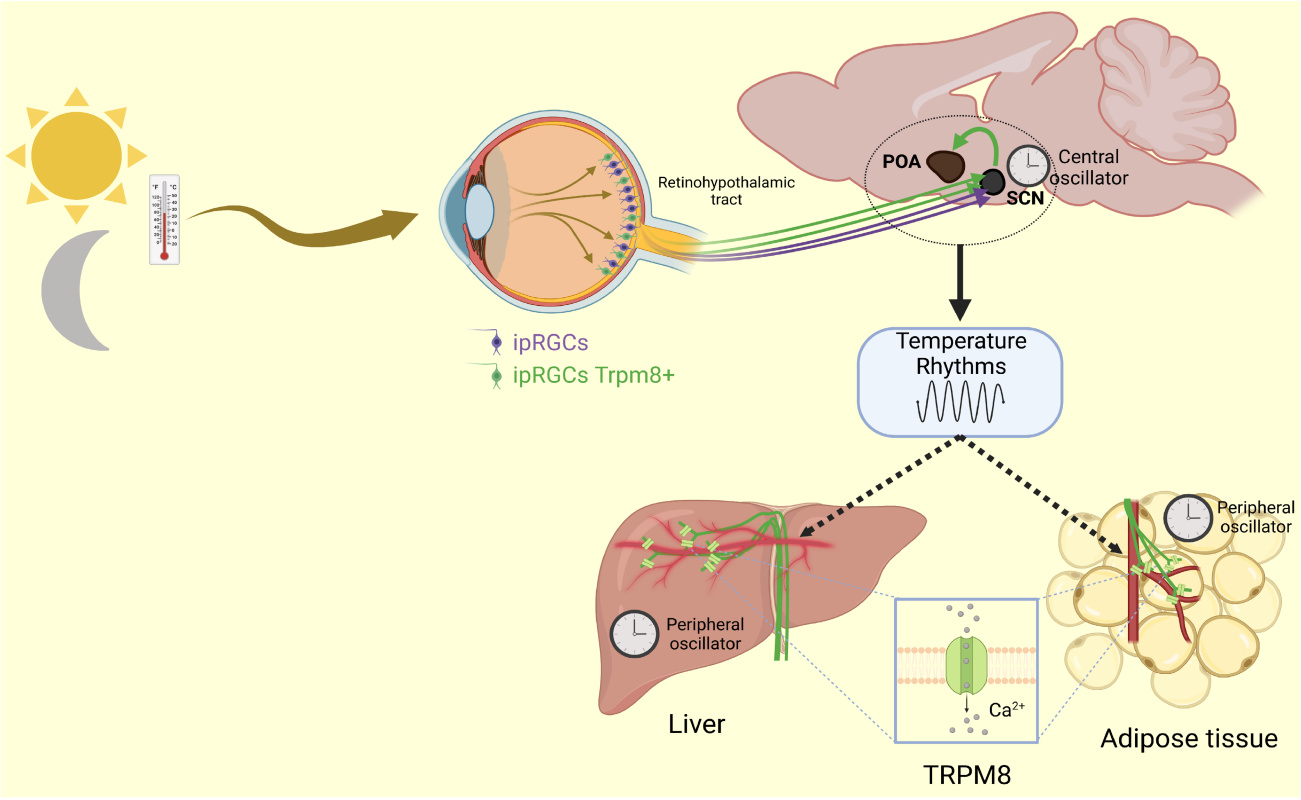

FIGURE 8 TRPM8 is expressed in a subset of retinal interneurons and ipRGC neurons projecting to the SCN, the master clock. The activity of TRPM8 fine tunes clockwork and neuropeptide levels in this hypothalamic nucleus, contributing to the regulation of the circadian oscillation of Tc. Tc fluctuations would be then detected by TRPM8 in peripheral organs, including liver and WAT, serving as entrainers for peripheral oscillators in these metabolic tissues.

EGFPf into the TRPM8 start codon was described previously[23] and homozygous *Trpm8*^{EGFPf} mice are null for TRPM8. To enhance EGFPf expression, the lox-P-flanked neomycin selection cassette introduced into the *Trpm8* locus during the generation of the transgene was excised.[27]

Experiments were performed with adult mice of both sexes of 3–10 months of age. In the experiments of immunofluorescence in the retina with the reporter line *Trpm8*^{EGFPf} we used mice at postnatal days 15 to 21 (P15-P21), because we observed that the levels of GFP expression in the retina of this transgenic mouse line were highest at the postnatal period. We made a great effort to have representative results from females and males in all experiments. But, in occasions, and depending mainly on availability, we had experiments with a predominance of animals of one sex.

For experiments, mice were housed at 21 ± 1°C, except that other temperature was indicated in the text. All animal procedures were approved by the local Ethics Committee on Animal Care at the University of Santiago de Compostela and the University Miguel Hernández of Elche and were conducted in accordance with European guidelines.

4.2 | RNA isolation and RT-PCR

Trigeminal ganglia (TG) and retina were isolated from C57BL/6J mice. RNA was extracted using TRIzol™ Reagent (Invitrogen) following the manufacturer's instructions. cDNA was synthetized using SuperScript™ III Reverse Transcriptase (Invitrogen) and random primers. For amplification, conventional PCR was performed using KAPA2G Fast DNA Polymerase (Sigma-Aldrich) with the following specific primers:

- Mouse TRPM8 forward 5′-GGAACTCCATGATGCATCTCTC-3′ and reverse 5′-GGGGATGATGAATAGACACAGG-3′ (amplicon 466 bp).
- Mouse Per2 forward 5′- ACACCACCCCTTACAAGCTTC-3 and reverse 5′- CGCTGGATGATGTCTGGCTC-3′ (amplicon 780).
- Constitutive gene HPRT forward 5′-CAGTCCCAGCGTCGTGATTA-3′ and reverse 5′-AGCAAGTCTTTCAGTCCTGTC-3′ (amplicon 169 bp).

To avoid genomic amplification, amplicons were designed to span introns. The products were visualized in a 1.5% agarose gel.

4.2.1 | Real-time PCR

Total RNA was isolated from mouse TG, and retina using TRIzol™ (Invitrogen). cDNA was synthesized with Transcriptor First Strand cDNA Synthesis Kit (Roche Diagnostics, Basel, Switzerland), and reactions of quantitative real-time PCR were done using iQ SYBR Green Supermix (Bio-Rad Laboratories, Alcobendas, Spain) on iCycler equipment (7500 PCR Systems, Applied Biosystems, Life Technologies, Carlsbad, USA). Samples were denatured at 95°C for 15 s, annealed at 58°C for 15 s, and extended at 72°C for 60 s for a total of 35 cycles. The samples were quantified using Sequence Detection Software 1.4 (Applied Biosystems), with HPRT as normalization control.

Specific primers:

- TRPM8 forward 5′-GTACATCTCTGAGCGCACCA-3′ and reverse 5′-CTCCTTGGGCAAAACACACG-3′ (amplicon 74 pb).
- Per2 forward 5′- CTCCAGCGGAAACGAGAACT-3′ and reverse 5′- GCTTTGGCAGACTGCTCACT-3′ (amplicon 195 pb).
- HPRT forward 5′-CAGTCCCAGCGTCGTGATTA-3′ and reverse 5′-AGCAAGTCTTTCAGTCCTGTC-5′ (amplicon 169 pb).

The results obtained were quantified using the $2^{-\Delta\Delta CT}$.

4.3 | Immunohistochemistry

4.3.1 | Immunofluorescence in reporter lines

Trpm8$^{BAC\text{-}EYFP}$ as well as homozygous *Trpm8*^{EGFPf} mice were used, females and males indistinctly. In the case of *Trpm8*$^{BAC\text{-}EYFP}$, we used adult mice (3–5 months of age). In *Trpm8*^{EGFPf} reporter mice we used mice at postnatal days 15 to 21 (P15-P21). Adult and young mice were anaesthetized with sodium pentobarbital (70 mg/Kg) and isoflurane respectively. Then, animals were perfused with 4% paraformaldehyde (PFA). Brain, liver, gonadal WAT and eyes were dissected and post-fixed in PFA at 4°C overnight. Eyes were post-fixed for only 4 h in 4% PFA at 4°C. After post-fixation, samples were stored in phosphate-buffered saline (PBS) at 4°C until processed.

Brains were sectioned on a vibratome (Leica, VT1000S) and 50- to 70-μm-thick sections were placed in a 96 well tissue culture plate with PBS. Some of the retinas were processed using a free-floating protocol as follows: tissues were rinsed twice in Tween-Tris Buffered Saline (TTBS, 0.05 M Tris Base, 0.9% NaCl, 0.05% Tween 20, pH 7.4) for 10 min and then incubated in Blocking Buffer solution (BB, 5% bovine serum albumin [BSA] in TTBS containing 1% Triton-X100) for 1 h at room temperature (RT). Next, samples were incubated in primary antibody solution

containing chicken anti-GFP antibody (1:2000, Abcam, ab13970, RRID: AB_300798) diluted in BB for 72 h (brain slices of *Trpm8*$^{BAC\text{-}EYFP}$ only overnight) at 4°C. This antibody recognizes both GFP and YFP. Samples were washed four times with TTBS for 15 min and incubated in secondary antibody solution containing donkey anti-chicken Alexa 488 antibody (1:800, Jackson ImmunoResearch 703-545-155, RRID: AB_2340375) diluted in BB for 48 h (brain slices of *Trpm8*$^{BAC\text{-}EYFP}$ only 2 h) at 4°C. Then, samples were washed four times with TTBS (15 min) and incubated for 5 min in Hoechst nuclear staining solution (0.5 μg/ml Hoechst 33342 [Invitrogen H1399] in PBS, pH 7.4). All these steps were performed in gentle agitation. Finally, samples were mounted onto microscope slides (Normax) with Fluoromount™ aqueous medium (Sigma). Some of the retinas were whole-mounted.

The rest of the tissues (liver, gonadal WAT, retinas) were processed using a slide-attached protocol as follows: samples were cryoprotected and stored until used in 30% sucrose in PBS with 0.01% sodium azide (Sigma-Aldrich S2002). Later, samples were embedded in immersion medium for cryogenic slides (CryoGlue, SLEE medical) in appropriate size moulds and quickly frozen in dry ice. Finally, samples were sectioned in a cryostat (MNT, SLEE medical) at 20–24 μm thickness and adhered to microscopic slides (Superfrost™ Adhesion Slides, Thermo Scientific). Samples were kept a 4°C until used. Slides were washed twice for 5 min with PBS-Tween (PBS-T, 0.1 M PBS, 0.05% Tween 20, pH 7.4). Then, slides were transferred to a wet chamber and incubated in BB for 1 h at RT. Next, samples were incubated with primary antibody solution containing chicken anti-GFP antibody (1:2000, Abcam, ab13970, RRID: AB_300798) diluted in BB at 4°C overnight. Then, slides were washed for 15 min (4 times) with PBT in gentle shaking and incubated with secondary antibody solution containing donkey anti-chicken Alexa 488 antibody (1:800, Jackson ImmunoResearch 703-545-155, RRID: AB_2340375) diluted in BB at 4°C for 2 h. Finally, slides were rinsed for 15 min (4 times) in PBT and stained with Hoechst nuclear staining solution (0.5 μg/ml Hoechst 33342 [Invitrogen H1399] in PBS, pH 7.4) for 5 min. Wash steps were made in gentle agitation. Finally, slides were mounted with Fluoromount medium (Sigma-Aldrich F4680). For retinal double immunostaining, the following primary antibodies were added: goat anti-ChAT antibody (1:250, Merck-Millipore AB144P, RRID: AB_2079751), or rabbit anti-melanopsin antibody (1:2500, ATS Bio AB-N398, RRID: AB_1608077). The following appropriate secondary antibodies were used: donkey anti-goat CFL555 (1:400, Santa Cruz Biotechnology sc-362265, RRID: AB_10989474) or goat anti-rabbit Alexa 594 (1:1000, Invitrogen A11012, RRID: AB_141359). For every experiment, some samples were processed without primary antibody as negative controls.

4.3.2 | Immunofluorescence of AVP in SCN

Brains were cut on a vibratome (Leica, VT1000S) and coronal sections of 50 μm were placed in a 96 well tissue culture plate with PBS. Sections including the suprachiasmatic nucleus of the hypothalamus were permeabilized with PBST and incubated with anti-AVP antibody (Millipore, PC234L), 1:1000 in Dako ChemMate antibody diluent (Dako, Glostrup, DK) overnight at 4°C. Then, sections were incubated with sheep anti-rabbit conjugated with cyanine 3 (Sigma-Aldrich) prepared at a dilution of 1:100, for 1 h. All dilutions were made in PBS (0.1 M phosphate, pH 7.4, containing 0.15 M NaCl). Between steps, sections were washed twice for 10 min each in the same buffer.

For quantification of AVP staining intensity, AVP immunofluorescence was visualized with a confocal microscope and then analysed off-line using the software Image J. The optical density (OD) of the staining intensity in the SCN was measured and subsequently normalized to the OD of adjacent background signal. To do that, a rectangle, with the same dimensions in each case, was drawn enclosing the specific signal and over adjacent brain areas of each section (background). We used 8–12 serial coronal sections for each animal. To ensure the analysis of comparable anatomic regions in all animals, sections were matched according to the Paxinos and Franklin's mouse brain atlas.[62] The mean of these 8–12 OD values was used as the densitometry value for each animal.

4.3.3 | Immunohistochemistry in rat retina

For TRPM8 immunohistochemistry in rat retinas, we used paraffin-embedded tissue. Animals were perfused, as stated above. Retina was removed from the ocular globe and embedded in paraffin. Thereafter, 5-μm-thick sections were cut with a microtome and placed on Superfrost Plus slides (Thermo Scientific). Slides were then deparaffinized before immunohistochemical techniques. A rabbit polyclonal antibody against TRPM8 (Abcam ab3243, RRID: AB_2208865) was used. Antigen retrieval was carried out using a microwave oven for 20 min at 750 W in 0.01 M TE Buffer (Tris 10 nM, EDTA 1 mM, pH 9). Slides were then tempered at RT for another 20 min and washed twice for 5 min with PBS. Slides were transferred to a wet chamber and consecutively incubated in: (1) polyclonal antibody anti-TRPM8 (1:5000) in antibody diluent (Dako Real, Agilent Technologies) overnight at RT, (2) 3% hydrogen peroxide (Merck) to block endogenous peroxidase (10 min), (3) goat anti-rabbit immunoglobulins conjugated to

peroxidase-labelled dextran polymer (Dako LSAB+ System-HRP, Agilent Technologies), (4) 3,3′-diaminobenzidine tetrahydrochloride (DAB, Sigma) solution prepared by diluting one DAB-buffer drop in 1 ml PBS (10 min) and (5) counterstain with Mayers haematoxylin for 1 min. Sections were dehydrated in ethanol, rinsed in xylol and mounted in a synthetic medium (Entellan® 107960, Sigma-Aldrich). Between steps, sections were washed twice for 5 min with PBS and after step 5 with water. Primary antibody specificity was tested by pre-adsorption with the immunogen peptides: peptide 1 H2N-RNQLEKYISERTIQD-OH and peptide 2 H2N-NDLKGLLKEIANKIK-OH (Abcam ab187961).

4.4 | Eye injection of fluorescent cholera toxin

Animals were anaesthetized with isoflurane (5% induction, 3% maintenance) and placed under a binocular scope. Then, a small hole was punctured at the corneal limbus with a 30-gauge needle. Through the hole, 1µl of 1% cholera toxin subunit B conjugated to Alexa Fluor 594 (Invitrogen C34777) in PBS was injected into each eye, with a fine glass micropipette connected to an aspirator mouth tube. Mice recovered from the procedure (2–3 min duration) on a heating pad set at 37°C. Seventy-two hours after injection, mice were perfused with 4% PFA and brains were processed using the free-floating section protocol described previously.

4.5 | Ocular temperature during a dynamic cold plate test

Ocular surface temperature was determined by IR thermography. Mice were placed individually on a metallic plate of 16.5 ×16.5 cm (Hot/Cold Plate, Bioseb, Vitrolles, France), surrounded by a methacrylate box. A high-resolution infrared camera (Avio InfReC Analyzer NS9500, Tokyo) was fixed frontally with a tripod. The plate was exposed to a descending temperature ramp (from 30 to 0°C, at a rate of 1°C/min) and a video of the animal was recorded at 48 frames per second during the whole assay (30 min). Temperature of each eye (Teye) was quantified offline using the software of the camera (InfReC Analyzer Pro). The highest Teye was selected for each animal when the plate temperature (Tplate) was 30, 25, 20, 15, 10 and 0°C.

4.6 | In situ hybridization

Mice coronal brain sections (16 µm thick), were cut on a cryostat and incubated with specific antisense oligodeoxynucleotides for *Per2 and AVP*:

- Per2: 5′- GCTCCTTCAGGGTCCTTATCAGTTCTTTGTGTGCGTCAGCTTTGG-3′.
- AVP: 5′- ACGAAGCAGCCCAGCTCGTCCGCGCAGCAGATGCTTGGTCCGAA-3′.

These probes were 3′-end labelled with[35] S-α-dATP using terminal deoxynucleotidyl transferase. The specificity of the probes was confirmed by incubating the sections with an excess of the unlabelled probes. In situ hybridizations were performed as previously described.[63,64] Briefly, frozen sections were fixed with 4% paraformaldehyde in 0.1 mol/L phosphate buffer (pH 7.4) at room temperature for 30 min. They were then dehydrated using 70%, 80%, 90%, 95% and absolute ethanol (5 min each). The hybridization was carried out overnight at 37°C in a wet chamber. Hybridization solution contained 1×10^6 cpm per slide of the labelled probe, 4× SSC (20× SSC: 3 mol/L sodium chloride, 0.3 mol/L sodium citrate, pH 7), 50% deionized formamide, 1× Denhardt's solution, 10% dextran sulphate and 10 µg/ml sheared, single-stranded salmon sperm DNA (all reagents from Sigma). Afterwards, the hybridized sections were sequentially washed in 1× SSC at room temperature, four times in 1× SSC at 42°C (30 min per wash), one time in 1× SSC at room temperature (1 h), and then rinsed in water and ethanol. Finally, the sections were air-dried and exposed to Hyperfilm β-Max (Amersham) at room temperature for 4 to 6 days.

Autoradiographic signals were scanned and then analysed using the open-source imaging software ImageJ. The OD of the hybridization signal was determined and subsequently normalized to the OD of its adjacent background value. To do that, a rectangle, with the same dimensions in each case, was drawn enclosing the specific hybridization signal and over adjacent brain areas of each section (background). To ensure the analysis of comparable anatomic regions in all animals, sections were matched according to the Paxinos and Franklin's mouse brain atlas.[62] We used 16–20 serial coronal sections for each animal (4 to 5 slides, 4 sections/slide). The mean of these 16–20 values was used as the densitometry value for each animal.

4.7 | Core body temperature (Tc) and motor activity determination

Core body temperature (Tc) and motor activity were measured using implantable radiotelemetric probes (G2 E-mitter series, MiniMitter, Starr Life Sciences; model ER-4000) and a VitalView telemetry system. Probes were surgically implanted in the peritoneal cavity under general anaesthesia with isoflurane. Animals recovered for 7 days in a room at 21°C, in 12 h light/12 h dark cycles with water and food ad libitum to ensure the absence of infection

or fever. During recording of data, individual mice were housed in plastic cages, with ~5 mm of bedding, on individual telemetric receivers (ER-4000, MiniMitter, Starr Life Sciences). Telemetric data from up to eight mice were recorded simultaneously and collected every 30 s using VitalView software (Starr Life Sciences).

To estimate the main parameters of Tc, including mean, minimum, maximum, amplitude and rising phase, the raw data (monitored over 3–4 days) were smoothed using a boxcar filter (width of 15 min) in Origin 8.6 software (Origin Lab). Mean daily profiles for each animal (as a function of ZT/CT) were determined. The amplitude of the diurnal rhythm in each individual was calculated as the difference between the highest and lowest values of these 24-h averages. Rising phase was estimated for each animal as the ZT/CT when the value of these 24-h averages first became higher than the overall daily mean Tc, as previously reported.[65] The former parameters were also estimated directly from raw records by fitting sinusoids. Values derived from these fits were similar to those estimated by the method described above. By convention, ZT0 corresponds to start of day (i.e. lights on) and ZT12 to start of night (i.e. lights off).

4.7.1 | Protocol of dark/dark and light/light experiments

Control and *Trpm8*$^{-/-}$ mice were housed in standard light/dark conditions (light/dark, 12 h/12 h) and then released in dark/dark or light/light conditions. The durations of constant darkness or constant light exposure are detailed in the text. Mice were housed at 29 or 21°C and Tc and motor activity was determined. Temperograms and actograms were generated using the ActogramJ plug-in in the open-source imaging software ImageJ, running on the Fiji platform.[66]

4.8 | Experimental design and statistical analysis

Data are represented as mean ± SEM. n represents the number of mice per group. For randomization, predefined numbers were assigned to each treatment group. The different experimental groups were processed identically throughout the whole experiment.

Statistical calculations were performed using the Statistical Package for Social Sciences (IBM) software (SPSS), GraphPad Prism 6.01 (GraphPad) and MATLAB. Before all statistical analyses, data were examined for assumptions of normality and equality of variance using the Kolmogorov–Smirnov test, followed by the Levene test. For the analysis of Tc and motor activity, we used the non-parametric Fisher's exact permutation test (MATLAB). Day/night or L/D, D/D and L/L results were analysed by two-way ANOVA with genotype and lighting conditions as main factors. A post hoc Bonferroni test was performed when there was a significant interaction between both main factors. Statistical significance between two groups was determined by an unpaired t test.

All material submitted is in accordance with good publishing practice in physiology.[67]

ACKNOWLEDGMENTS

The first three authors (AR, CF-P and PO) contributed equally to this manuscript and are allowed to re-order the sequence of the first authors to reflect this if needed in, for example, their CVs. The authors are grateful to L. Casas, M. Espinosa, M. Tora, E. Quintero and A. Miralles for their excellent technical assistance.

FUNDING INFORMATION

This study was supported by the Projects RT2018-099995-B100 to RS and AEI/10.13039/501100011033 to FV (Spanish Ministry of Science and Innovation), co-financed by Generalitat Valenciana (PROMETEO/2021/031) and the Severo Ochoa Programme for Centres of Excellence in R&D (ref. SEV-2017-0723). PO held predoctoral fellowship of MINECO (BES-2011-047063). AR holds a Margarita Salas post-doctoral fellowship (Spanish Ministry of Universities).

CONFLICT OF INTEREST

The authors declare no competing financial interests.

ORCID

Alfonso Reimúndez https://orcid.org/0000-0003-1675-5267
Carlos Fernández-Peña https://orcid.org/0000-0002-0726-3204
Pablo Hernández-Ortego https://orcid.org/0000-0001-9591-4144
Rosalía Gallego https://orcid.org/0000-0002-6015-4680
Francisco Martín-Cora https://orcid.org/0000-0001-8620-0588
José Luís Pardo-Vázquez https://orcid.org/0000-0003-4623-2440
Lindsay A. Schwarz https://orcid.org/0000-0002-0613-5518
Félix Viana https://orcid.org/0000-0003-1439-949X
Rosa Señarís https://orcid.org/0000-0002-4536-2609

REFERENCES

1. Pittendrigh CS. Temporal organization - reflections of a darwinian clock watcher. *Annu Rev Physiol*. 1993;55:16-54.

2. Dibner C, Schibler U, Albrecht U. The mammalian circadian timing system: organization and coordination of central and peripheral clocks. *Annu Rev Physiol*. 2010;72:517-549.
3. Mohawk JA, Green CB, Takahashi JS. Central and peripheral circadian clocks in mammals. *Annu Rev Neurosci*. 2012;35:445-462.
4. Ashton A, Foster RG, Jagannath A. Photic entrainment of the circadian system. *Int J Mol Sci*. 2022;23(2):729.
5. Berson DM, Dunn FA, Takao M. Phototransduction by retinal ganglion cells that set the circadian clock. *Science*. 2002;295(5557):1070-1073.
6. Provencio I, Jiang G, De Grip WJ, Hayes WP, Rollag MD. Melanopsin: an opsin in melanophores, brain, and eye. *Proc Natl Acad Sci U S A*. 1998;95(1):340-345.
7. Hattar S, Liao HW, Takao M, Berson DM, Yau KW. Melanopsin-containing retinal ganglion cells: architecture, projections, and intrinsic photosensitivity. *Science*. 2002;295(5557):1065-1070.
8. Bass J. Circadian topology of metabolism. *Nature*. 2012;491(7424):348-356.
9. Cox KH, Takahashi JS. Circadian clock genes and the transcriptional architecture of the clock mechanism. *J Mol Endocrinol*. 2019;63(4):R93-R102.
10. Jin XW, Shearman LP, Weaver DR, Zylka MJ, De Vries GJ, Reppert SM. A molecular mechanism regulating rhythmic output from the suprachiasmatic circadian clock. *Cell*. 1999;96(1):57-68.
11. Guzmán-Ruiz MA, Ramirez-Corona A, Guerrero-Vargas NN, et al. Role of the suprachiasmatic and arcuate nuclei in diurnal temperature regulation in the rat. *J Neurosci*. 2015;35(46):15419-15429.
12. Barrett RK, Takahashi JS. Temperature compensation and temperature entrainment of the chick pineal cell circadian clock. *J Neurosci*. 1995;15(8):5681-5692.
13. Brown SA, Zumbrunn G, Fleury-Olela F, Preitner N, Schibler U. Rhythms of mammalian body temperature can sustain peripheral circadian clocks. *Curr Biol*. 2002;12(18):1574-1583.
14. Herzog ED, Huckfeldt RM. Circadian entrainment to temperature, but not light, in the isolated suprachiasmatic nucleus. *J Neurophysiol*. 2003;90(2):763-770.
15. Lahiri K, Vallone D, Gondi SB, Santoriello C, Dickmeis T, Foulkes NS. Temperature regulates transcription in the zebrafish circadian clock. *PLoS Biol*. 2005;3(11):2005-2016.
16. Prolo LM, Takahashi JS, Herzog ED. Circadian rhythm generation and entrainment in astrocytes. *J Neurosci*. 2005;25(2):404-408.
17. Kornmann B, Schaad O, Bujard H, Takahashi JS, Schibler U. System-driven and oscillator-dependent circadian transcription in mice with a conditionally active liver clock. *PLoS Biol*. 2007;5(2):179-189.
18. Poletini MO, Moraes MN, Ramos BC, Jerônimo R, Castrucci AML. TRP channels: a missing bond in the entrainment mechanism of peripheral clocks throughout evolution. *Temperature*. 2015;2(4):522-534.
19. Ruby NF, Burns DE, Heller HC. Circadian rhythms in the suprachiasmatic nucleus are temperature-compensated and phase-shifted by heat pulses in vitro. *J Neurosci*. 1999;19(19):8630-8636.
20. Buhr ED, Yoo S-H, Takahashi JS. Temperature as a universal resetting cue for mammalian circadian oscillators. *Science*. 2010;330(6002):379-385.
21. George R, Stanewsky R. Peripheral sensory organs contribute to temperature synchronization of the circadian clock in Drosophila melanogaster. *Front Physiol*. 2021;12:622545.
22. Bautista DM, Siemens J, Glazer JM, et al. The menthol receptor TRPM8 is the principal detector of environmental cold. *Nature*. 2007;448(7150):204-208.
23. Dhaka A, Murray AN, Mathur J, Earley TJ, Petrus MJ, Patapoutian A. TRPM8 is required for cold sensation in mice. *Neuron*. 2007;54(3):371-378.
24. Reimúndez A, Fernández-Pena C, García G, et al. Deletion of the cold thermoreceptor TRPM8 increases heat loss and food intake leading to reduced body temperature and obesity in mice. *J Neurosci*. 2018;38(15):3643-3656.
25. Ordás P, Hernández-Ortego P, Vara H, et al. Expression of the cold thermoreceptor TRPM8 in rodent brain thermoregulatory circuits. *J Comp Neurol*. 2021;529(1):234-256.
26. Señarís R, Ordás P, Reimúndez A, Viana F. Mammalian cold TRP channels: impact on thermoregulation and energy homeostasis. *Pflügers Arch*. 2018;470(5):761-777.
27. Dhaka A, Earley TJ, Watson J, Patapoutian A. Visualizing cold spots: TRPM8-expressing sensory neurons and their projections. *J Neurosci*. 2008;28(3):566-575.
28. Masland RH. The tasks of amacrine cells. *Vis Neurosci*. 2012;29(1):3-9.
29. Famiglietti EV Jr. 'Starburst' amacrine cells and cholinergic neurons: mirror-symmetric on and off amacrine cells of rabbit retina. *Brain Res*. 1983;261(1):138-144.
30. Reiner A, Fitzgerald MEC, Del Mar N, Li C. Neural control of choroidal blood flow. *Prog Retin Eye Res*. 2018;64:96-130.
31. Cohen GY, Ben-David G, Singer R, et al. Ocular surface temperature: characterization in a large cohort of healthy human eyes and correlations to systemic cardiovascular risk factors. *Diagnostics*. 2021;11(10):1877.
32. Naidorf-Rosenblatt H, Landau-Part D, Moisseiev J, et al. Ocular surface temperature differences in retinal vascular diseases. *Retina*. 2022;42(1):152-158.
33. Yan L, Takekida S, Shigeyoshi Y, Okamura H. Per1 and Per2 gene expression in the rat suprachiasmatic nucleus: circadian profile and the compartment-specific response to light. *Neuroscience*. 1999;94(1):141-150.
34. Tominaga K, Shinohara K, Otori Y, Fukuhara C, Inouye SIT. Circadian-rhythms of vasopressin content in the suprachiasmatic nucleus of the rat. *Neuroreport*. 1992;3(9):809-812.
35. Chou C-F, Zhu X, Lin Y-Y, Gamble KL, Garvey WT, Chen C-Y. KSRP is critical in governing hepatic lipid metabolism through controlling Per2 expression. *J Lipid Res*. 2015;56(2):227-240.
36. Destici E, Jacobs EH, Tamanini F, Loos M, van der Horst GTJ, Oklejewicz M. Altered phase-relationship between peripheral oscillators and environmental time in Cry1 or Cry2 deficient mouse models for early and late chronotypes. *PLoS One*. 2013;8(12):e83602.
37. McKemy DD, Neuhausser WM, Julius D. Identification of a cold receptor reveals a general role for TRP channels in thermosensation. *Nature*. 2002;416(6876):52-58.
38. Peier AM, Moqrich A, Hergarden AC, et al. A TRP channel that senses cold stimuli and menthol. *Cell*. 2002;108(5):705-715.
39. Takashima Y, Daniels RL, Knowlton W, Teng J, Liman ER, McKemy DD. Diversity in the neural circuitry of cold sensing revealed by genetic axonal labeling of transient receptor potential melastatin 8 neurons. *J Neurosci*. 2007;27(51):14147-14157.

40. O'Malley DM, Masland RH. Co-release of acetylcholine and gamma-aminobutyric acid by a retinal neuron. *Proc Natl Acad Sci U S A*. 1989;86(9):3414-3418.
41. Parver LM. Temperature modulating action of choroidal blood flow. *Eye (Lond)*. 1991;5(Pt 2):181-185.
42. Tamai K, Toumoto E, Yamada K, Ogura Y. Effects of irrigation fluid temperature on choroidal circulation during vitrectomy. *Curr Eye Res*. 1999;18(4):249-253.
43. Alcalde I, Íñigo-Portugués A, González-González O, et al. Morphological and functional changes in TRPM8-expressing corneal cold thermoreceptor neurons during aging and their impact on tearing in mice. *J Comp Neurol*. 2018;526:1859-1874.
44. Shen WL, Kwon Y, Adegbola AA, Luo J, Chess A, Montell C. Function of rhodopsin in temperature discrimination in drosophila. *Science*. 2011;331(6022):1333-1336.
45. Beaule C, Houle LM, Amir S. Expression profiles of PER2 immunoreactivity within the shell and core regions of the rat suprachiasmatic nucleus - lack of photic entrainment and disruption by constant light. *J Mol Neurosci*. 2003;21(2):133-147.
46. Morin LP. SCN organization reconsidered. *J Biol Rhythms*. 2007;22(1):3-13.
47. Welsh DK, Takahashi JS, Kay SA. Suprachiasmatic nucleus: cell autonomy and network properties. *Annu Rev Physiol*. 2010;72:551-577.
48. Schwartz WJ, Coleman RJ, Reppert SM. A daily vasopressin rhythm in rat cerebrospinal-fluid. *Brain Res*. 1983;263(1):105-112.
49. Kalsbeek A, Buijs RM, Engelmann M, Wotjak CT, Landgraf R. In-vivo measurement of a diurnal-variation in vasopressin release in the rat suprachiasmatic nucleus. *Brain Res*. 1995;682(1–2):75-82.
50. Maruyama T, Ohbuchi T, Fujihara H, et al. Diurnal changes of arginine vasopressin-enhanced green fluorescent protein fusion transgene expression in the rat suprachiasmatic nucleus. *Peptides*. 2010;31(11):2089-2093.
51. Moraes MN, Monteiro de Assis LV, Henriques FS, Batista ML Jr, Guler AD, de Lauro Castrucci AM. Cold-sensing TRPM8 channel participates in circadian control of the brown adipose tissue. *Biochim Biophys acta, Mol. Cell Res*. 2017;1864(12):2415-2427.
52. Buijs FN, Leon-Mercado L, Guzman-Ruiz M, Guerrero-Vargas NN, Romo-Nava F, Buijs RM. The circadian system: a regulatory feedback network of periphery and brain. *Phys Ther*. 2016;31(3):170-181.
53. Saini C, Morf J, Stratmann M, Gos P, Schibler U. Simulated body temperature rhythms reveal the phase-shifting behavior and plasticity of mammalian circadian oscillators. *Genes Dev*. 2012;26(6):567-580.
54. McCoy DD, Zhou L, Anh-Khoi N, Watts AG, Donovan CM, McKemy DD. Enhanced insulin clearance in mice lacking TRPM8 channels. *Am J Physiol Endocrinol Metab*. 2013;305(1):E78-E88.
55. Fonfria E, Murdock PR, Cusdin FS, Benham CD, Kelsell RE, McNulty S. Tissue distribution profiles of the human TRPM cation channel family. *J Recept Signal Transduct Res*. 2006;26(3):159-178.
56. Rossato M, Granzotto M, Macchi V, et al. Human white adipocytes express the cold receptor TRPM8 which activation induces UCP1 expression, mitochondrial activation and heat production. *Mol Cell Endocrinol*. 2014;383(1–2):137-146.
57. Jiang C, Zhai M, Yan D, et al. Dietary menthol-induced TRPM8 activation enhances WAT 1C "browning 1D" and ameliorates diet-induced obesity. *Oncotarget*. 2017;8(43):75114-75126.
58. Bishnoi M, Kondepudi KK, Gupta A, Karmase A, Boparai RK. Expression of multiple transient receptor potential channel genes in murine 3T3-L1 cell lines and adipose tissue. *Pharmacol Rep*. 2013;65(3):751-755.
59. Wang Y, Leung VH, Zhang Y, et al. The role of somatosensory innervation of adipose tissue. *Nature*. 2022;609(7927):569-574.
60. de la Peña E, Mälkiä A, Varas H, Caires R, et al. The influence of cold temperature on cellular excitability of hippocampal networks. *PLoS One*. 2012;7(12):e52475.
61. Morenilla-Palao C, Luis E, Fernández-Peña C, et al. Ion channel profile of TRPM8 cold receptors reveals a role of TASK-3 potassium channels in thermosensation. *Cell Rep*. 2014;8(5):1571-1582.
62. Paxinos G, Franklin KBJ. *The Mouse Brain in Stereotaxic Coordinates*. 5th ed. Academic Press; 2019.
63. López M, Seoane LM, Tovar S, et al. A possible role of neuropeptide Y, agouti-related protein and leptin receptor isoforms in hypothalamic programming by perinatal feeding in the rat. *Diabetologia*. 2005;48:140-148.
64. Trujillo ML, Spuch C, Carro E, Senarís R. Hyperphagia and central mechanisms for leptin resistance during pregnancy. *Endocrinology*. 2011;152(4):1355-1365.
65. Knight EM, Brown TM, Gümüsgöz S, et al. Age-related changes in core body temperature and activity in triple-transgenic Alzheimer's disease (3xTgAD) mice. *Dis Model Mech*. 2013;6(1):160-170.
66. Schmid B, Helfrich-Förster C, Yoshii T. A new ImageJ plug-in "ActogramJ" for chronobiological analyses. *J Biol Rhythms*. 2011;26(5):464-467.
67. Jensen BL, Persson PB. Good publication practice in physiology 2021. *Acta Physiol (Oxf)*. 2022;234:e13741.

SUPPORTING INFORMATION

Additional supporting information can be found online in the Supporting Information section at the end of this article.

How to cite this article: Reimúndez A, Fernández-Peña C, Ordás P, et al. The cold-sensing ion channel TRPM8 regulates central and peripheral clockwork and the circadian oscillations of body temperature. *Acta Physiol*. 2023;237:e13896. doi: 10.1111/apha.13896